Exploring the potential of luminescence methods for dating Alpine rock glaciers

Fuchs, Margret C ; Böhlert, Ralph ; Krbetschek, Matthias ; Preusser, Frank ; Egli, Markus

DOI: https://doi.org/10.1016/j.quageo.2013.07.001

Exploring the potential of luminescence methods for dating Alpine rock glaciers

Margret C. Fuchs[1]*, Ralph Böhlert[2], Matthias Krbetschek[3], Frank Preusser[4], Markus Egli[2]

[1]Institute of Geology, TU Bergakademie Freiberg, Bernhard-von-Cotta-Strasse 2, 09596 Freiberg, Germany

[2]Department of Geography, University of Zurich, 8057 Zurich, Switzerland

[3]Senckenberg Museum of Mineralogy and Geology Dresden, Section Luminescence, c./o. Institute of Applied Physics, TU Bergakademie Freiberg, Leipziger Str. 23, Freiberg 09596, Germany; deceased, October 15th 2012

[4]Department of Physical Geography and Quaternary Geology, Stockholm University, 10691 Stockholm, Sweden

*corresponding author: fuchsm@student.tu-freiberg.de

Abstract

Rock glaciers contain valuable information about the spatial and temporal distribution of permafrost. The wide distribution of these landforms in high mountains promotes them as useful archives for the deciphering of the environmental conditions during their formation and evolution. However, age constraints are needed to unravel the palaeoclimatic context of rock glaciers, but numerical dating is difficult. Here, we present a case study assessing the potential of luminescence techniques (OSL, IRSL) to date the inner sand-rich layer of active rock glaciers. We focus on the signal properties and the resetting of the signal prior to deposition by investigating single grains. While most quartz shows low signal intensities and problematic luminescence characteristics, K-feldspar exhibits much brighter and well-performing signals. Most signals from plagioclases do not show suitable properties. Luminescence signals far below saturation indicate distinct but differential bleaching. The finite mixture model was used to determine the prominent populations in the equivalent dose distributions. The luminescence ages represent travel times of grains since incorporation into the rock glacier and hence, minimum ages of rock glacier formation. Luminescence ages between 3 ka and 8 ka for three rock glaciers from the Upper Engadine and Albula region (Swiss Alps) agree well with independent age estimates from relative and semi-quantitative approaches. Therefore, luminescence seems to have the potential of revealing age constraints about processes related to the formation of rock glaciers, but further investigations are required for solving some of the problems remaining and reducing the dating uncertainties.

Keywords: Rock glacier, luminescence dating, OSL, IRSL, single grains, Alps

1. Introduction

In order to set modern climate-related observations into long-term perspectives, environmental proxies recorded in various natural archives are needed to reconstruct past climate and landscape evolution. In mountain areas, highly climate sensitive glacial and periglacial processes are the main agents modulating the Earth's surface. These regions are also of special interest because within short horizontal distances they host climatic regimes similar to those of widely separated latitudinal belts (Beniston et al., 1997; Beniston, 2005). The resulting sensitivity to changes in environmental conditions constitutes mountain areas to be among the key regions for observing, reconstructing, and finally predicting climate change and its impact on surfaces processes.

Extensive areas of high mountain regions are governed by permafrost conditions with rock glaciers marking the lower boundary of its distribution (Haeberli et al., 2011). Rock glaciers comprise perennially frozen and ice-rich debris on non-glaciated mountain slopes that creep steadily under the influence of gravity (e.g., Haeberli et al., 2006). Active rock glaciers of the Alps (i.e. containing ice and actively deforming) are assumed to have formed and evolved during the Holocene (Frauenfelder et al., 2005). Relict forms at lower altitudes have lost their ice content and do not creep anymore. As they initially must have formed under permafrost conditions, they have a considerable potential for constraining past climatic conditions (Ballantyne et al., 2009). However, the deciphering of rock glaciers as geo-archives requires a temporal assignment by means of numerical dating.

Haeberli et al. (2003) suggest a concept of combined relative and (semi)quantitative techniques for rock glacier dating. Photogrammetric measurements of surface flow fields, weathering rinds, Schmidt-hammer rebound, and lichenometry indicate increasing surface ages towards the front. Extrapolation of present day velocities may indicate surface ages of 5 – 6 ka (Kääb et al., 1998) or 3 – 5 ka (Frauenfelder et al., 2005), but with uncertainties related to possible changes in palaeo-velocities or even phases of flow inactivity. Although the relative and semi-quantitative approaches confirm the concept of rock glaciers developing at millennial time scales, spatial variations in flow velocities indicate various site-specific effects (e.g., local slopes, ground temperature, rock types). This emphasises that the interpretation of relative age constraints and their comparison between study sites requires calibration based on numerical dating. Radiocarbon dating of the only organic remnants encountered during drilling at the Murtel rock glacier yielded a ^{14}C age of 2.3 $\pm$ 0.1 ka BP (Haeberli et al., 2003). From the rock glaciers Murtèl, Muragl and La Veduta (Upper Engadine, Switzerland) preliminary results indicate problematic luminescence properties due to low signal intensities in quartz (90–200 µm fraction). Although no detailed data sets are presented, Haeberli et al. (2003) state that all datable samples give ages between about 4 and 8 ka. Böhlert et al. (2011) suggest two different permafrost activity phases since the Lateglacial: one phase after the ice retreat following the Younger Dryas and the other in the Holocene. Based on cosmogenic nuclide dating and weathering rinds in the French Alps, Cossart et al. (2010) distinguished three main generations of rock glaciers since the Lateglacial: the first one around 11 or 12 ka, the second around 2 or 3 ka, and the last one in more recent times.

Over the last decades, advances in optically stimulated luminescence (OSL) and infrared stimulated luminescence (IRSL) techniques broadened the field of applications in sediment dating (e.g., Lian and Roberts, 2006; Bateman, 2008; Fuchs and Owen, 2008). The main advantages are that these methods

93 directly date the material's last light exposure associated to the timing of deposition, and that they use
94 almost ubiquitously present quartz (OSL) and feldspar (IRSL) for dating. Concerning the dating of rock
95 glaciers, luminescence techniques are not reliant on organic material necessary for radiocarbon dating,
96 and are independent of stable surfaces as required for cosmogenic nuclide dating. However, the OSL
97 properties of quartz, the mineral chosen in most applications, are often problematic in mountainous areas
98 (e.g., Preusser et al., 2006; Steffen et al., 2009). This is apparently related to the fact that OSL signals
99 suitable for dating result from sensitisation during repeated sediment transport/deposition cycles (Pietsch
100 et al., 2008; Jeong and Choi, 2012), but with the exact physical processes in the crystal lattice being
101 poorly understood (cf. Preusser et al., 2009). This problem is not known to apply for feldspars, but the
102 signal of this mineral can be less stable, and such fading of the signal can cause underestimation of the
103 determined age (Wintle, 1973). Furthermore, the IRSL signal from feldspar is expected to bleach more
104 slowly than the OSL from quartz (e.g., Wallinga, 2002a).
105 In the context of glacial and periglacial environments and their related transport processes, it has to be
106 considered that insufficient light exposure may not completely bleach the pre-existing luminescence
107 signals (cf. Fuchs and Owen, 2008). Such incomplete bleaching causes residuals that form part of the
108 measured signal and, if not detected and excluded, lead to an overestimation of the palaeodose and,
109 accordingly, of the calculated age. However, it has been shown that poorly bleached sediments are
110 usually composed of grains with different bleaching levels (Duller, 1994). It is possible to detect
111 differential bleaching when measuring the signal of small aliquots or single grains, where it is expressed
112 by the spread of replicate measurements (cf. Wallinga, 2002b; Duller, 2008). Statistical approaches are
113 then applied to extract the true burial dose (e.g., Galbraith et al., 1999; Bailey and Arnold, 2006). To
114 ensure a correct extraction of the well-bleached signal portion, such approaches have to account for
115 sample specific parameters that have an effect on the expected spread of data without differential
116 bleaching (e.g., instrumental error, material-inherent variability, microdosimetry).
117 In this study, we investigate the potential of both, quartz OSL and feldspar IRSL (K-feldspar, plagioclase)
118 focussing on single grain measurements to date three active rock glaciers in the Piz Julier area and in the
119 Val Tschitta, Swiss Alps (Fig. 1). For the Gianda Grischa and the Suvretta rock glacier age estimates are
120 available from streamline interpolations and relative dating measurements (Frauenfelder et al., 2005).
121 Due to the relatively simple geometry and the availability of relative age estimates, the Salteras rock
122 glacier was chosen as an additional site. Firstly, we describe rock glacier sedimentary dynamics and
123 discuss the relevance of processes involved in grain input and transport within rock glaciers for the

interpretation of luminescence ages. Secondly, we present the luminescence signals of quartz OSL and feldspar IRSL measurements and statistically analyse the dose distributions for prominent populations. Finally, we discuss the derived grain travel times in the context of the process related assumptions and accordingly the potential of luminescence techniques to constrain the age of rock glacier formation.

2. Methodological aspects of rock glacier dating

2.1. Formation and dynamics of rock glaciers

According to Barsch (1996) three main aspects define active rock glaciers: the form of a lobate or tongue-shaped body, the perennially frozen unconsolidated material supersaturated with interstitial ice and ice lenses, and the process of down-slope creep as a consequence of deforming ice contained in them (cohesive flow). Berthling (2011) emphasises the cumulative deformation by long-term creep of ice/debris mixtures under permafrost conditions. All rock glaciers studied in this work formed in crystalline areas and can be described as 'bouldery rock glaciers' with mean boulder diameters of ≥ 15-20 cm (Böhlert, 2010), following the classification scheme of Matsuoka et al. (2005). They are furthermore classified as valley floor/tongue shaped rock glaciers according to Humlum (1982) and Hamilton and Whalley (1995).

Rock glaciers form when the ice content of perennially frozen debris or talus on slopes exceeds saturation, and the body of debris and ice starts deforming slowly (creeps) under gravitational stress (Haeberli et al., 2006). Such creeping, ice-rich rock glacier bodies develop at slopes where a concave area favours the accumulation of material from adjacent steep bedrock walls (Fig. 2). The processes leading to material and ice accumulation are numerous, and complex interactions with glaciers are possible (Haeberli et al., 2006), sometimes making a clear identification of the landform challenging (Böhlert, 2010; Berthling, 2011). For instance, the source material can be provided by ice-cored moraines ('moraine-derived' rock glaciers) or by debris flows and solifluction. Separation processes result in the typical sorting of grain sizes, represented by boulder enrichment in the top and bottom layer whereas the fine-grained material concentrates in the inner part. The upper, normally boulder-enriched part represents a highly heterogeneous layer that is strongly influenced by the thickness and temporal distribution of the snow cover (Haeberli et al., 2006). Characteristic active layer thicknesses range from a few centimetres to a few metres (Humlum, 1997). In the fine-grained (Fig. 2 and 3) and often ice supersaturated material of the inner parts energy fluxes are mainly conduction-controlled. The creep of rock glaciers can be

155 described by ‘caterpillar-like’ flow behaviour (Fig. 2): boulders at the surface fall down at the over-
156 steepened front and are subsequently overridden by ice-supersaturated, fine-grained material.
157
158 2.2. Sediment dynamics and relevance for luminescence dating
159 According to the model of rock glacier dynamics described above, the material available for dating
160 derives either from the upper boulder-rich layer, principally suitable for cosmogenic nuclide dating, or
161 from the inner fine-grained layer that has the potential to be dated by luminescence methods. The
162 ‘caterpillar-like’ flow results in an age inversion of the boulder enriched layers: at the surface, the age of
163 the blocky material increases towards the front, while for the overridden base-layer the opposite applies
164 (Haeberli, 1985; Fig. 2). Beside inaccessibility of the oldest boulders in the base layer, additional
165 problems for numerical dating (i.e. cosmogenic nuclides) are related to the unstable exposure of boulder
166 surfaces and possible inheritance of cosmogenic nuclides from previous exposure. The layer of fine-
167 grained material at the front of active rock glaciers represents buried particles of the long-term creeping,
168 perennially frozen talus (Haeberli et al., 2003, Fig. 3). Dating this inner, fine-grained layer will give the
169 time when grains were incorporated into the rock glacier. As a consequence, luminescence ages of such
170 layers will represent travel times, i.e. the time since the signal was reset during deposition on the rock
171 glacier surface followed by shielding and signal growth as long as grains are transported within the rock
172 glacier body.
173 In this context, two main processes need to be considered regarding their effects on the luminescence
174 signal: (1) grain pathways into the rock glacier with corresponding characteristic bleaching history, and (2)
175 grain transport within the rock glacier body affecting sediment mixing and signal growth. It is important to
176 note that luminescence ages, due to the input paths of fine-grained material described above, will likely
177 only represent the minimum age of the rock glacier. Only in the case of dominant material input and
178 sufficient bleaching at the rock glacier’s rooting zone, undisturbed signal growth during grain transport
179 towards the front, and under the assumption that no fine grained material is eroded at the front, the travel
180 time might indicate the age of rock glacier formation.
181 Possible process-related effects on the luminescence signal are summarized in Table 1. The accurate
182 determination of the travel time fundamentally relies on the level of signal resetting prior to grain
183 incorporation, related to how the fine-grained material was supplied to and incorporated into the rock
184 glacier. Different input pathways lead to distinct populations of grains with characteristic bleaching
185 histories and potentially representing different times of incorporation. In principal, material available for

rock glacier aggregation may be derived from headwall erosion of bedrock that surrounds the rooting zone, from aeolian sediment supply, from basal uptake or from internal grain size reduction. The short transport distances from surrounding headwalls might cause incomplete bleaching, while prolonged surface retention times of grains due to, for example, perennial snowfields or avalanche residues as well as aeolian input will likely deliver well-bleached grains. Potential sources of incompletely bleached grains are basal uptake of material and internal, permafrost-related grain size reduction resulting from the shear stress of creeping, ice super-saturated sediment.

After incorporation into the rock glacier, luminescence signals are expected to reveal an age-distance relation with increasing signal towards the front of the rock glacier (Fig. 3), but sediment mixing might disturb this simple relation. Causes for vertical and lateral sediment mixing might be related to gravitational creeping permafrost and corresponding uncertainties in grain trajectories. Possible mechanisms of vertical sediment mixing involve melt-water that may transfer grains from the surface of the rock glacier into deeper parts. The input of material along crevasses (extension/compression zones) similarly promotes the vertical and lateral mixing of surface-derived grains with older sediment layers.

Apart from uncertainties due to the grain pathways, processes related to the gravitational creep of ice super-saturated material might cause variations in the efficiency of the dose rate and with regard to the shielding against cosmic radiation. Potential microdosimetric variations mainly relate to uncertainties in the water/ice content and especially in its distribution. Ice super-saturation, segregated ice or ice lenses can cause inhomogeneity in the distribution of radionuclides in the fine-grained matrix and may affect the actual dose rate of each individual grain.

Considering the possibility of both, different input-related bleaching histories and transport-related sediment mixing, we expect to measure luminescence signals that reveal different grain populations within the same sample. The determination of the travel time of grains from the mixed grain populations requires the correct detection and exclusion of signals from subsequently incorporated younger grains (age underestimation) and grains incompletely bleached prior to burial (age overestimation). The accurate and precise determination of the well-bleached grain population relies on reliable luminescence properties (e.g. dose-response relation, signal sensitivity and reproducibility) and at least some grains completely zeroed before incorporation into the rock glacier. Because the material loss at the rock glacier front is difficult to evaluate, the travel times based on the well-bleached grain population represent minimum ages of the rock glacier formation. To reduce the relative contribution of the external dose rates and related uncertainties to the total dose rate, we aim at comparing the results for three minerals with

differing internal dose rates (quartz, K-feldspar, and plagioclase; cf. Barre and Lamothe, 2010).

3. Study sites

The study sites are located in the eastern part of Switzerland (Upper Engadine). Greenish 'Albula Granite' comprised of quartz, plagioclase (in places altered to epidote), K-feldspar, biotite and rarely hornblende is the dominant rock type in the area (cf. Bearth et al., 1987). The reconstructed Last Glacial Maximum (LGM) ice surface geometry shows that the area was situated near the 'Engadine ice dome'. Trimline and other erosional features indicate that during the LGM the Albulapass formed a northward transfluence with ice flowing from the Engadine into the Rhine river system (Florineth, 1998; Florineth and Schlüchter, 2000; Bini et al., 2009). As a result of the highly unstable climate during the Lateglacial (c. 19-11.5 ka) and the early Holocene, a variety of climate-related landforms developed in mountain areas of the Alps. A geomorphic map of the region describes the landforms and the different glacier stages after the LGM (Maisch, 1981). The glacier stages were numerically dated measuring in-situ produced ^{10}Be in boulders on moraines, polished bedrocks, and roches moutonnées (Ivy-Ochs et al., 1996; Böhlert et al., 2011a,b). Distinct glacier stages could be attributed to the Daun (Oldest Dryas) phase (14.9 ± 1.8 ka) and several Egesen phases (Younger Dryas). At high-elevation sites near the LGM trimline, ^{10}Be exposure ages of glacially modified bedrock are between 11.2 ka and 13.5 ka (Böhlert et al., 2011a). This suggests the persistence of long-lasting small local ice caps after the breakdown of the LGM ice domes or, alternatively, a reformation of ice perhaps during the Younger Dryas. Exposure ages from a glacially polished rock barrier showed that this area was ice-free at the end of the Younger Dryas (9.0 ± 0.7 ka and 11.9 ± 0.9 ka; Böhlert et al., 2011a). In general, two different altitudinal levels of rock glaciers are recognised. A first generation (inactive rock glaciers) reaches altitudes down to 2000 – 2300 m asl. A second generation (active rock glaciers) is usually above 2400 – 2700 m asl (depending on exposure). Surface exposure dating (SED) of a roches moutonnées using ^{10}Be, ^{14}C dating of a peat bog, palynological investigations as well as glaciomorphologic mapping (Maisch, 1981) delimited the maximum age of the Lateglacial permafrost activity that apparently started shortly after the Younger Dryas (about 11.6 ka; Böhlert et al., 2011c). Soil analyses support these time constraints for the second activity phase that hypothetically started sometime around 6 ka ago and continues today (Böhlert et al., 2011c).

Three active rock glaciers were investigated (Fig. 1). Age constraints from relative and semi-quantitative methods, summarised in Frauenfelder et al. (2005), enable to set the here-measured luminescence ages

248 into context. Age estimations mainly based on streamline interpolations were the reason for the choice of
249 the Gianda Grischa and the Suvretta rock glacier. A comparably simple geometry in combination with a
250 dataset from relative dating approaches was the reason for the choice of the Salteras rock glacier as an
251 additional site. The sampling sites on each rock glacier are shown in Figure 4.
252
253 *Suvretta*
254 The Suvretta rock glacier is characterised by a more than 1 km long, relatively thin monomorphic body
255 creeping out of the cirque below the Piz Albana, in closest vicinity to Piz Julier (Fig. 1 and 4a). It covers
256 an altitudinal range of about 500 m, with a starting zone at around 2800 m and a front position at 2300 m.
257 The rock glacier front is undercut by the mountain stream coming down the Suvretta valley (Vonder
258 Mühll, 1993). The thickness of the permafrost body ranges from almost 100 m in the upper part to around
259 20 m near the front, as determined by geoelectric techniques. Active layer thickness does usually not
260 exceed 2 m (Vonder Mühll, 1993). The length profile is S-shaped: The slightly dipping root zone changes
261 at 2600 m to a steep zone of extending flow in the middle part, flattening again towards the valley bottom
262 with a zone of compressing flow in the tongue area. The area around the rock glacier was most probably
263 not influenced by extensive ice during the end of the Lateglacial and the Holocene (Suter, 1981;
264 Ohlendorf, 1998). The corresponding sheet from the Siegfried map (sheet St. Moritz, 1875) does not
265 indicate that the cirque was occupied by ice masses during the Little Ice Age (LIA). However, the
266 presence of (perennial) ice or snow patches cannot be ruled out.
267 Photogrammetric techniques determined horizontal surface displacement rates of up to 2 m a^{-1} and a
268 surface age at the front of approximately 3 ka (Kääb et al., 1997, 1998; Frauenfelder et al., 2005).
269 Reconstructed streamlines represent the trajectories of individual particles on the surface. Considering
270 that the overall advance rate of the rock glacier can be much smaller, the calculated ages have to be
271 interpreted as minimum ages. The maximum age (travel time) can be 2-5 times higher (Kääb, 2005). Both
272 Schmidt-hammer rebound values ‘r’ (Castelli, 2000) and weathering rind thicknesses (Laustela et al.,
273 2003) show a clear trend following the length profile and, in combination with the estimated ages from
274 photogrammetry, allows for calibration. The oldest parts near the tongue yielded weathering rind
275 thicknesses between 2.5 and 3 mm and r-values ranging around 35, respectively (Frauenfelder et al.,
276 2005). The values are typical for rock glaciers having a maximum surface age of several thousand years
277 that suggest Holocene rock glacier formation (Böhlert et al., 2011c).
278

279 *Gianda Grischa*

280 The double-tongued Gianda Grischa rock glacier (Figs. 1 and 4b) on the western slopes of Piz Julier is,
281 from a geometrical point of view, the most complex one. Multiple generations of lobes with different
282 activity stages are distinguishable. Several situations show younger active parts overrunning older
283 inactive or even relict parts. This is especially pronounced at the orographic left tongue. In order to
284 reduce complexity, we chose the right tongue for sampling. The southern margin of the middle part of the
285 rock glacier is steeply sloping down towards SW, in Figure 4b identifiable as a bright area clearly
286 contrasting the more gently sloping surface of the rock glacier.

287 To the north of this active polymorphic rock glacier an inactive exemplar can be separated. Its location in
288 a flat niche was occupied by a small glacier during the LIA, while the cirque of the active rock glacier was
289 ice-free at this time (Coaz, 1850; Siegfried map, sheet St. Moritz, 1875). According to Suter (1981), well-
290 pronounced Egesen-equivalent moraines near Julierpass indicate a glaciation during the Younger Dryas.
291 Two-dimensional electrical resistivity tomography (ERT) surveys showed unusual high active layer
292 thicknesses up to 4 to 5 m. Typical values in this region are 3 to 3.5 m on rock glaciers and 4 to 5 m in
293 rock walls. Photogrammetry yields lower surface displacement rates compared to the rock glacier
294 Suvretta, with an average velocity of 0.4 to 0.5 m a^{-1} and maximum values around 0.8 m a^{-1}. The
295 minimum estimated surface age is 4 to 5 ka (Frauenfelder et al., 2005). Schmidt-hammer measurements
296 show no clear trend. This may be a result of boulders being rearranged under the influence of gravity in
297 the steep part of the rock glacier, causing a reset of the 'clock' (Frauenfelder et al., 2005). Weathering
298 rinds, however, show a development with increasing thicknesses towards the front, at least on the
299 orographic left side (Laustela, 2003). Maximum values (median, mode) are in the range of 1.5 to 2 mm.
300 This trend is not as clear on the orographic right side, but the measured values are in the same range,
301 indicating a similar age structure on both sides. Related to the age estimation, rind growth rates are about
302 half as high as in the case of the rock glacier Suvretta, although made up of the same source material
303 (Frauenfelder et al., 2005).

304

305 *Salteras*

306 The Salteras rock glacier, originating from the NE-oriented cirque to the east of Piz Salteras, shows a
307 rather simple geometry without zones of pronounced compressing or extending flow. The long profile is
308 slightly convex with an increasing slope angle towards the tongue, which is about to creep over a steep
309 grassy slope. The front is thereby divided into two individual lobes. In front of the talus apron, several

vegetation covered lobe-shaped forms are visible (Fig. 4c). These might be interpreted as remnants (ridges in a compressing zone or front?) of a collapsed relict form, indicating that the rock glacier Salteras has experienced several activity phases. Lacking lichen coverage and weakly consolidated coarse blocks covering the surface suggest an active stage of the rock glacier.

Neither Schmidt-hammer r-values nor modal values of weathering rind thicknesses – both measured in the middle and the lower part of the rock glacier (Laustela, 2003) – show a clear trend representing an increasing exposure time to weathering processes towards the front. The high r-values (45 to 50) agree with the very thin and often completely absent weathering rinds. Using the median, there is a trend indeed; still, the values are very small (< 1 mm). This picture of surprisingly fresh and unweathered surface material might be explained by the influence of glacier ice that might have removed the more weathered rocks at the surface. Although the Siegfried map (sheet Savognin, 1887) shows no ice in this position, moraines found in the upper part support the conclusion that at least the upper parts of the rock glacier have been covered by surface ice during the LIA (Maisch, 1981).

4. Methods

4.1. Sampling

Rock glaciers were sampled at the talus apron at the front (Fig. 4). To avoid the influence of superficially eroded and reworked material, we chose sampling spots in the upper third of the slope, clearly higher than the visible debris accumulation zones in the lower parts, but below the coarse blocks at the surface. The approximately 40° steep slopes showed a low stability. Digging was carried out whenever possible underneath isolated boulders that protected the sandy matrix to a certain degree from collapsing immediately. Keeping a minimum distance of 40 cm from the boulder itself, approximately 50-100 cm of the surface material was removed until fresh sediment was reached. During sampling, an opaque cover served for shielding the sediment from daylight. Horizontal sediment cores were recovered in opaque plastic cylinders and properly sealed for transportation and storage. The surrounding sediment was sampled for gamma-spectrometric analyses of the sediment's radionuclide content.

4.2. Determination of dose rate

The radionuclide content of the sediment was determined based on the specific activities of ^{238}U, ^{232}Th and of ^{40}K and daughters by means of low level HPGe gammaspectrometry. Radioactive disequilibria in

341 the ^{238}U-series were evaluated by comparing the specific activities of subsequent radionuclides with focus
342 on ^{222}Rn daughters to identify Rn-loss. The cosmic dose rate was estimated according to latitude,
343 longitude, mean altitude (accounting for the altitude change during grain transport from the source to
344 talus apron) and thickness of the debris coverage above sampling positions. The dose rate efficiency was
345 corrected based on the mineral and sediment density, grain-size, etched layer, and by the assumed
346 palaeowater content. The palaeowater content refers to the measured in situ content compared to
347 saturation values. While the in situ values are attributed to conditions near the front during sampling
348 season, the sample's water saturation provides a reference for previously higher water/ice contents
349 required for the creep process of the rock glacier. Potential uncertainties arise from inhomogeneity in the
350 sediment matrix and distribution of ice (e.g., ice lenses), although the creep process might average out
351 corresponding dose rate variations between grains. To account for the expected high palaeowater
352 content up to super-saturation (associated to actively creeping rock glaciers), the used palaeowater
353 values was set to about two third of the saturation values. To cover possible variations in water content,
354 high errors were included that range from in situ and exceed saturation values.
355 The parameters contributing to the total external dose rates of the three rock glaciers are given in Table
356 2. No significant disequilibria are indicated for ^{238}U due to the specific activities of the Rn daughters ^{214}Pb
357 and ^{214}Bi. A lower activity of ^{210}Pb compared to the rest of the decay chain was observed for samples
358 GiG1 and 2, but the effect on age calculation is less than 1%. For the determination of the mineral-
359 internal dose rate of K-feldspars, a potassium content of 12.5 ± 0.5% was assumed (Huntley and Baril,
360 1997) and for plagioclase 2.0 ± 0.8% (cf. Barre and Lamothe, 2001). Investigations on samples from the
361 Swiss lowland reveal very little variation in the internal K-content of K-feldspars (D. Gaar, pers. com.)
362 Based on the measured specific activity of the sediment, the estimated cosmic component and correction
363 parameters the overall environmental dose rate (and luminescence age) was calculated with the ADELE
364 software (Kulig, 2005). The age and uncertainty calculation follows the principles described by Aitken
365 (1985).
366
367 *4.3. Sample preparation*
368 In the laboratory, the samples were treated under attenuated red light. The two outermost centimetres of
369 the sediment cores were removed on each side as these parts could have experienced light exposition
370 during sampling. This material was used to determine the water content (in situ and saturation) of the
371 sample. The material from the inner part of the cylinders was used for the separation of the quartz and

372 the feldspar grains. Sieving isolated the 100 - 200 µm grain size fractions for multiple-grain aliquot and
373 200–300 µm for single grain measurements. The treatment with 10% HCl and 30% H_2O_2 removed
374 carbonates and organic matter, respectively. To assure the separation of quartz, K-feldspar and
375 plagioclase, we introduced a feldspar flotation before density separation. The feldspar flotation was
376 carried out in a solution of 0.2% HF with pH 2.4 - 2.7 to activate feldspar adherence to bubbles that were
377 induced by pumping air through a frit and the foam agent dodecylamine. Both, the enriched quartz and
378 the feldspar froth, were washed in 5% HCl and then separated due to density with sodium polytungstate
379 (quartz: 2.62 - 2.67 g cm^{-3}; K-feldspar: <2.58 g cm^{-3}; plagioclase: 2.58 - 2.62 g cm^{-3}). The quartz fraction
380 was then etched using 40% HF for 60 min and the feldspar fraction using 10% HF for 40 min to remove
381 ~10 µm of the outer, alpha-ray affected rim of the grains. The following cleaning with 37% HCl (quartz)
382 and 10% HCl (feldspars) washed out the fluorite precipitates. Final sieving isolated the fractions 90–160
383 µm for multiple-grain aliquots and 200 - 250 µm for single grain analyses. The multiple-grain aliquots
384 were prepared by fixing homogenised subsamples of the separated material on aluminium discs within a
385 diameter of 4 mm using silicon oil. Such an aliquot will contain about 200 - 400 grains, of which a small
386 amount will be luminescent (cf. Heer et al., 2012). For single grain measurements, discs with 100 holes
387 arranged in a grid were used, each dimensioned to accommodate a single grain of the size 200 - 250 µm
388 (Bøtter-Jensen et al., 2000).
389
390 *4.4. OSL measurements of quartz*
391 OSL multiple-grain aliquots measurements were carried out using a Risø TL/OSL reader DA 20 equipped
392 with a Sr-90 beta irradiator (5.6 Gy min^{-1}). OSL emission was stimulated with blue LEDs (470 nm) for 50 s
393 at 125 °C and detected through a U 340 Hoya optical filter. 20 aliquots of samples SAL1 and SUV2 were
394 measured following the single-aliquot regenerative-dose (SAR) protocol (Murray and Wintle, 2000) for
395 quartz. Subsequent to the natural signal, the aliquot-specific dose-luminescence relation was determined
396 based on six regeneration cycles including monitoring of recuperation, recycling ratio, and sensitivity
397 change. Preheat before each OSL stimulation was set to 260 °C and cutheat to 220 °C for 10 s (for
398 details on measurement parameters, see supplementary material D). For both samples, four additional
399 dose recovery tests (Murray and Wintle, 2003) were applied to assess the reproducibility of OSL signals
400 in reference to a known laboratory dose. This coefficient of variation (v_{DR}) determines the sample-specific
401 variability of OSL signals inherited from the sample's material and the applied measurement conditions.

Additionally, single grain measurements were performed for samples SAL1, SUV1–4 and GiG1–2 to avoid the averaging effect of luminescence signals from multiple grain aliquots (e.g., Duller, 2008). Single grain measurements improve the distinction between different populations in the dose distribution and allow for assessing the degree of bleaching. Using a Risø TL/OSL Reader DA 15, luminescence emission was stimulated by a green laser (532 nm, ~50 Wcm^{-2}) for 2 s at 125 °C and detected through a Hoya U 340 filter. For each sample 2–4 discs were measured. For technical reasons, it was not possible to fill the discs (100 grains) completely. Grain counting under the microscope after the measurement confirmed the degree of filling per disc to be 70 - 90%. Equivalence doses were determined following the SAR protocol and parameters described above (for details see supplementary material D). Dose recovery tests were carried out only for SAL1.

4.5. IRSL measurements of feldspars

IRSL single grain measurements were carried out for K-feldspars (samples SAL1, SUV2–4, GiG1–2). Additionally, plagioclase was measured for SAL1 and SUV4 to test their applicability for dating with respect to the lowered potassium content and corresponding contribution to the internal dose (cf. Barre and Lamothe, 2010). The Risø TL/OSL DA 20 reader was equipped with an IR single grain stimulation unit and we used stimulation with an IR laser (830 nm, 150 mW) for 5 s at 30 °C.

Suitable conditions for luminescence emission and detection were evaluated for sample SAL1 by carrying out thermal transfer tests for different pre-heat temperatures (220, 240, 260 and 280°C for 10 s) and by applying different detection filters (280, 410, 560 nm). The measurement procedure followed the SAR protocol of Murray and Wintle (2000), but by replacing measurement of the natural signal by measurement of a laboratory bleached (zero dose) sample. Thermal transfer is expressed by the equivalent dose determined by the SAR measurement (three aliquots for each pre-heat level). This procedure was repeated for each filter, which corresponds to the three typical IRSL emission wavebands of feldspars with different properties (Krbetschek et al., 1997). According to the results from the thermal transfer tests (Fig. 5), pre-heat temperature and optical detection filter were set to 280°C and 410 nm, respectively. Although the signals determined through the 410 nm optical filter are similar to slightly lower for the preheat temperature of 220°C, corresponding errors suggest less appropriate measurement conditions for both, 10% as well as 90% LED power. Generally higher thermal transfer and much higher errors in equivalent dose estimation were detected through the 280 nm and especially through the 560

nm optical filter. Dose recovery tests according to Murray and Wintle (2003) were performed for SAL1 (K-feldspar, plagioclase) and SUV2 (K-feldspar).

Anomalous fading is often considered to ubiquitously cause systematic underestimation of IRSL ages (e.g., Huntley and Lamothe, 2001). However, it has been shown that IRSL emission centred at 410 nm (used in our study) is less affected by fading than UV emissions (Krbetschek et al., 1997). In particular for the Alps several studies have shown that IRSL ages agree well with independent age control (Preusser et al., 2001, 2003; Preusser and Schlüchter, 2004;). Storage tests used for correcting the signal loss have recently shown to yield IRSL ages that are overestimating independent age control (Gaar and Preusser, 2012; Lowick et al., 2012). Furthermore, it has been shown that the fading rate is probably temperature dependent (Thomsen et al., 2008) and Krause et al. (1997) did not observe fading in their samples from Antarctica. Considering all the above, we refrained from carrying out time-consuming storage tests, especially since it would have been very challenging to simulate the permafrost environment of our samples.

4.6. Analyses of luminescence data

The adequacy of detected luminescence signals for further analyses was evaluated based on their signal intensities above background (shine down curves) and dose-signal relation (growth curves) using the software ANALYST 3.24 (Duller, 2007). The distribution of equivalent doses for each sample is then analysed using the R software and the R package Luminescence (Kreutzer et al., 2012) in order to assess the degree of differential bleaching and presence of distinct signal populations.

For well-bleached samples, a normal distribution of equivalent doses is expected, with standard deviations corresponding to uncertainties in individual doses and in dose rates. The palaeodose calculation based on the arithmetic mean or using the central age model (CAM; Galbraith et al., 1999) is sufficient. Non-normal distributions and higher standard deviations indicate differential bleaching and hence, require statistical modelling to determine the palaeodose that represents the true burial time of the well-bleached grains (e.g., Olley et. al., 1998; Bailey and Arnold, 2006). The minimum age model (MAM) is designed to determine the palaeodose from skewed dose distributions assuming values from well-bleached grains for the lower portion of the distribution (Galbraith et al., 1999). However, the MAM is very sensitive to the lowermost equivalent doses. In the case of sediment mixing with younger grains the use of the MAM might be problematic. For rock glaciers, the grain input processes with differential bleaching and the potential of transport-related sediment mixing suggests that the dose distributions may be

463 composed of several distinct populations. Accordingly, the finite mixture model (FMM; Galbraith and
464 Green, 1990) is preferred to determine the dominant population of the sample.
465 The overdispersion constitutes the essential input parameter for both, the MAM and the FMM. We have
466 no appropriate material (e.g., well-bleached aeolian sand from the study area) to assess the
467 overdispersion of our samples independently. Arnold et al. (2007) and Arnold and Roberts (2009) found
468 values between 0.1 and 0.4 for fluvial deposits from different geographical regions. Accordingly, we
469 tested the effect of using different overdispersion values (0.05 - 0.50) on the performance of the FMM
470 (details are given in the supplementary material). Due to the overall low variations in FMM results with
471 changes in overdispersion, a value of 0.3 seems to be a reasonable approximation for our samples,
472 which also represents the value found for samples from the Swiss lowlands (Gaar and Preusser, 2012).
473

474 ## 5. Results

475

476 *5.1. Signal properties of quartz OSL*

477 In general, the analysed material often shows problematic luminescence properties and the low
478 intensities often hardly allow separating the luminescence signal from the background noise. The very
479 few equivalent doses (cf. Table 3) of SUV1 (n=3), SUV2 (n=1), SUV4 (n=3), GiG1 (n=5), and GiG2 (n=2)
480 that could reliably be determined, provide only limited information about the dose distribution. For such
481 samples, single grain measurements are not adequate enough to allow for the identification of distinct
482 equivalent dose populations and the degree of bleaching. Corresponding dose-response curves from
483 Suvretta and Gianda Grischa show a variable correlation of the OSL signal and applied laboratory dose
484 (Fig. 6; top and middle). Poor recycling ratios and pronounced sensitivity changes and recuperation
485 indicate poor luminescence properties of the measured material. Much brighter signals reveal higher
486 luminescence sensitivities and low errors in equivalent dose estimation for several grains from Suvretta
487 and most grains from Salteras (Fig. 6; bottom). The high uncertainties in recovering applied laboratory
488 doses indicate material-inherent uncertainties that affect the reproducibility of OSL signals. Recovered
489 doses deviate from the applied dose by more than 30% in both, multiple-grain aliquot (SAL1) and single
490 grain (SAL1) measurements. The latter tends to underestimate the recovery dose (Fig. 7a).
491

492 *5.2. Signal properties of feldspar IRSL*

493 Luminescence signals of IRSL single grain measurements show generally higher intensities for K-
494 feldspar compared to plagioclase (Fig. 8). More grains reveal initial IRSL signals above the generally
495 elevated background noise of 500 – 1000 counts per 0.01s. Dose-response curves from the majority of
496 those grains suggest a reliable dose-signal correlation. Recycling ratios close to unity and low
497 recuperation allowed for an improved curve fitting. Dose recovery tests for K-feldspar reproduce the
498 applied laboratory dose with a variation (v_{DR}) of 8.1% for SAL1 (Fig. 7b). In the case of plagioclases
499 (SAL1), the overestimation of the applied laboratory dose resulted also in a high v_{DR} (~85%). The poor
500 reproducibility complicates the interpretation of equivalent doses. Only few equivalent doses could be
501 determined from measured plagioclase grains (SAL1, SUV4). Low signal intensities and large
502 uncertainties in growth curve fitting indicate mostly poor luminescence properties.
503
504 *5.3. Analyses of equivalent dose distributions*
505 The generally large scatter of equivalence doses (Fig. 9 - 11) implies a heterogeneous composition of the
506 distributions, caused by insufficient bleaching and/or resulting from factors connected to the sediment
507 dynamics within the rock glaciers. Hence, further statistical treatment is needed to infer palaeodoses
508 representing the true age of incorporation. A major problem in our study is the fact that in several cases
509 the luminescence properties described above lead to only few determined values per sample along with
510 high uncertainties (Table 3). This complicates or even precludes the analyses of the equivalent dose
511 distributions; such limited data sets do not allow drawing conclusions about the bleaching level. We used
512 the arithmetic mean (as a pragmatic solution) in a descriptive sense but did not calculate luminescence
513 ages for these samples.
514 Only samples where more than 15 equivalent doses could be determined were used for further statistical
515 analyses (Fig. 9 - 11). Well suited in this context is the Salteras sample (SAL1, Fig. 9) for which a large
516 number of K-feldspar single grain (n=74) and quartz single grain (234) equivalent dose values are
517 available. Additionally, we have a sufficient number of multiple-grain quartz measurements (18) for this
518 sample (Table 3). For Suvretta (Fig. 10), only four out of nine different measurements yielded sufficient
519 numbers of equivalent dose vales: SUV1 multiple-grain quartz (18), SUV2 single grain K-feldspar (60),
520 SUV3 single grain quartz (58), and SUV4 single grain K-feldspar (35). For Gianda Grischa (Fig. 11), only
521 GiG2 single grain K-feldspar (43) gave rise to a substantial number of analysable measurements (Table
522 3). For all of these samples, we observe a broad spread of equivalent dose values, in many cases with
523 relative standard deviations above 100%. The CAM yields overall lower values compared to simply using

524 the arithmetic mean and thus, may be less affected by outliers (Table 3). However, the CAM values do
525 not represent the main cluster at the lower end of the dose distribution as indicated by the probability
526 density function (PDF) of most samples (Fig. 9 - 11). The MAM palaeodose calculation tends to
527 underestimate the main data cluster (maximum in PDF). Especially single low values affect MAM
528 calculations, in some cases leading to palaeodose estimation based on only the lowest 1-5 values. The
529 FMM enables a robust determination of the dominant population, corresponding to the main data cluster
530 at the lower end of the dose distribution. Using the overdispersion value of 0.3, we determined two to
531 three components in our samples. In all our samples the highest proportion (for most samples >70%) is
532 represented by the lowest component, except for SAL 1 OSL multiple grain analysis with the second as
533 the main component (Tab. 3). In most cases, the main component is accompanied by a secondary
534 component of ~10-30%. For a few samples a minor third component of <10% could be distinguished
535 comprising the highest dose values. Only for SAL 1 multiple grain OSL this minor component comprises
536 the lowest equivalent doses. Two samples (SUV 2 and GiG 2 single grain IRSL, both K-feldspar) differ
537 from that picture by revealing two prominent components, of which the lower one is slightly dominant
538 (>50%) and the secondary (<50%) indicates a distinct population of higher dose values.
539
540 *5.4. OSL and IRSL ages*
541 Table 3 summarises the calculated luminescence ages for samples that allowed statistical analyses
542 based on more than 15 values. All ages represent the main dose population determined by the FMM. The
543 well performing luminescence signals of the Salteras rock glacier revealed ages of 6.4 ± 1.2 ka and 6.4 ±
544 0.6 for multiple grain quartz and single grain K-feldspar, respectively. Although the age of 7.7 ± 0.7 ka for
545 single grain quartz is slightly higher, it confirms the overall consistency of the results of the investigated
546 luminescence signals. The less well performing plagioclase single grain signals do not allow for a robust
547 palaeodose and hence, age calculation. However, detectable equivalent doses and corresponding
548 arithmetic mean are similar to the other luminescence measurements. The consistency of the quartz and
549 K-feldspar ages indicates that anomalous fading is likely not affecting the samples under consideration.
550 For the rock glacier Suvretta (Table 3), we determine consistent ages of 5.2 ± 0.8 ka (multiple-grain
551 quartz) and 4.8 ± 0.5 ka (single grain K-feldspar) for the sample SUV2. Unfortunately, the OSL single
552 grain measurements of SUV2 were not successful. All approaches failed for close-by SUV1 apart from
553 three OSL single grain results that indicate significantly higher values. The laterally displaced samples
554 SUV3 and SUV4 revealed ages of 3.5 ± 0.5 ka (single grain quartz) and 3.0 ± 0.6 ka (single grain K-

feldspar), respectively. The OSL quartz and IRSL K-feldspar single grain datasets from SUV3 and SUV4 that consisted only of <15 values cover a comparable dose range like the FMM estimates of the robust datasets (>15 values). IRSL plagioclase measurements for SUV4 were not able to provide a sufficient dataset.

The sediments taken from the Gianda Grischa rock glacier yielded the poorest luminescence properties. Only for the single grain K-feldspar of sample GiG2, a substantial number of equivalent dose values are available (43), delivering an age of 3.0 ± 0.4 ka. Interestingly, the eight single grain K-feldspar values from sample GiG1 agree with the FMM results of GiG2. In contrast, OSL single grain measurements of both samples yielded only few values with significantly higher doses. The poorly constrained quartz signals prevent reliable age estimation.

6. Discussion

The problematic luminescence properties of quartz and feldspars, especially plagioclase, indicate overall low luminescence sensitivities of the sampled rock glacier material, typical for sediments that underwent no or only few sedimentation cycles (cf. Pietsch et al., 2009). While very low signal intensities are especially encountered with the quartz measurements, also feldspar measurements often show high uncertainties in dose response curves and partly poor reproducibility in the dose recovery tests. In general, the quartz OSL properties of the Salteras sample appear to be far more reliable than those of Suvretta and Gianda Grischa. A similar trend is observed for K-feldspar single grain measurements for Salteras compared to Suvretta and Gianda Grischa. We assume that material intrinsic properties of source rock play an important role for the differences in luminescence behaviour of the investigated rock glaciers. Although the rock type is everywhere similar, some minor differences in the mineral assemblage (and mineral structure) might exist (see also Böhlert et al., 2011a,b).

The equivalent doses indicate heterogeneous, in most cases positively skewed distributions that suggest differential bleaching. However, considering the possibility of different grain transport pathways along with sediment mixing, different grain populations may be present. While the MAM tends to underestimate the main signal cluster, palaeodose calculation based on the FMM seems to be more adequate to address both, differential bleaching as well as the possibility of the incorporation of surface-derived grains. For most samples, the main FMM component (>70%) represents the prominent signal cluster at the lower range of values that indicates a distinct population of well-bleached grains. Hence, we assume sufficient light exposure of grains during a dominating input process. Interestingly, we observe several rounded

586 grains under the microscope implying the presence of an aeolian component in the sediment matrix. The
587 secondary FMM component of ~10-30% comprises higher equivalent dose values accompanied in some
588 cases by an additional third component of <10% for highest values (Tab. 3), but the effects of incomplete
589 bleaching cannot be differentiated from the contribution of sediment mixing. For SUV 2 and GiG 2 single
590 grain IRSL, the prominent secondary FMM component of 40 – 47% may indicate a distinct input/uptake of
591 an older grain population. Single low values may relate to a minor influence of mixing. The FMM
592 distinguishes only for SAL 1 multiple grain OSL a minor component (<10%) from lowest equivalent doses.
593 However, further implications on grain input and transport process for individual dose populations remain
594 unresolved in our data set.
595 Dose rate analyses did not reveal any significant disequilibrium in the ^{238}U decay series from direct Rn
596 daughters. More challenging is the estimation of the palaeowater/ice content. The very low in situ
597 contents are associated to the summer conditions during the sampling season and are probably not
598 representative for the entire transfer time. Considering that creeping permafrost requires a high ice
599 content, values close to saturation are more likely representing the average during grain travel. To cope
600 with these overall uncertainties, large uncertainties for water content values have been included in this
601 study. Theoretically, high ice content and ice lenses may have caused an inhomogeneous distribution of
602 dosimeter minerals (quartz, feldspar) and radionuclides (radiation sources controlling signal growth) in the
603 sediment. However, measuring three minerals of different internal dose rates does not reveal systematic
604 effects according to the reduced influence of external microdosimetric variations of K-feldspars compared
605 to plagioclase and quartz. Overall, samples having a sufficient data set showed a clearly dominant cluster
606 that suggests normal distribution and only a low variation within the main population of assumed well-
607 bleached grains. It appears that the creeping process of rock glacier material results in a more or less
608 constant displacement of grains within the sediment-ice matrix, leading to an averaging effect on dose
609 rates.
610 The calculated luminescence ages represent the time since grains were incorporated into the rock glacier
611 and transported towards the talus front. Therefore, they provide minimum age of rock glacier formation.
612 Despite difficult material properties, the ages calculated by different approaches (Table 3) are consistent
613 for individual sampling sites. However, estimates differ between the different rock glaciers. The longest
614 grain travel times have been determined for Salteras. Compared to Suvretta and Gianda Grischa, this
615 could indicate differences in creeping rates. Additionally, the deviation of results from two laterally distant
616 sites at Suvretta implies that it might be even possible to resolve variations in creeping rates for distinct

lateral zones of rock glaciers. To confirm creeping rate differences, additional test are required that address the partly high luminescence variability encountered in dose recovery tests.

All luminescence ages for the currently still active rock glaciers are between 3 ka and 8 ka, supported by previous estimates (Haeberli et al., 2003) and in agreement with flow trajectory analyses and photogrammetric approaches that indicate minimum surface ages between 3 and 6 ka (Kääb et al., 1998; Frauenfelder et al., 2005). This confirms the concept of Holocene rock glaciers developing at millennial time scales as also deduced from weathering rinds, lichenometry and radiocarbon dating (Haeberli et al., 2003). Although derived travel times determine a similar time range as preliminary results of quartz measurements (4 – 8 ka) for the rock glaciers Murtèl, Muragl and La Veduta (Upper Engadine, Switzerland), results cannot be compared in terms of their reliability due to unavailability of measurement details.

However, the OSL based travel times from Salteras, Suvretta and Gianda Grischa indicate differences between the rock glaciers. Recent velocities measured at various sites reveal variations between and within rock glaciers that depend especially on slope, local climate and related ice content as well as temperature (Haeberli et al., 2003; Frauenfelder et al., 2005). Accordingly, the different travel times may simply reflect site-specific variations in flow velocities. To clearly distinguish rock glacier generations from travel times requires further investigations on the respective roles of different flow velocities and activity phases. Overall, the OSL based travel times need to be regarded as minimum ages and indicate that the investigated high Alpine rock glaciers began to evolve during the Early and/or Middle Holocene.

7. Conclusions

This is the first study systematically exploring the potential of luminescence dating of sediments that are imbedded in rock glaciers. In general, poor luminescence properties of both feldspar and, in particular, of quartz were encountered, with only some measurement approaches resulting in robust datasets. Most reliable results were yielded for Salteras, whereas samples from Suvretta and especially Gianda Grischa are highly problematic. Promising is the fact that most datasets showed a clear signal clustering at the lower end of the dose distribution, suggesting sufficient bleaching during a dominant grain input process, likely through aeolian sediment supply to and/or grain retention at the rock glacier surface. The heterogeneous dose distributions also indicate a contribution of incompletely bleached grains, but only limited effects of sediment mixing.

The luminescence ages are consistent at each individual sampling site, but show variations between rock glaciers and may indicate even differences between different parts of the same rock glacier lobe (Suvretta). Again, it should be noted that the ages represent the travel times of grains and hence represent only minimum ages of rock glacier formation. Luminescence ages between 3 ka and 8 ka fall within the expected time range determined by other relative and semi-quantitative approaches, indicating that rock glaciers started their present phase of activity in the Early/Middle Holocene. While the derived minimum ages do not further narrow down onset of rock glacier formation, they deliver valuable constraints about grain travel times and, hence, dynamics of rock glacier material. However, several questions about variations in luminescence properties and dose rates of sediments with high ice content have not been investigated here in detail, and need to be addressed in future studies.

Acknowledgements

This study was supported by the Swiss National Science Foundation grant numbers 20-109565/1 and 20-124380. We gratefully thank Alexandra Hilgers for the support and opportunity of OSL single grain measurements at the luminescence laboratory at the University of Cologne. We also received substantial support from Thomas Rosenberg during the IRSL single grain measurements at the luminescence laboratory of the University of Bern.

References

Aitken, M.J., 1985. Thermoluminescence dating. Academic Press, London, 359 pp.

Arnold, L.J., Roberts, R.G., 2009. Stochastical modelling of multi-grain equivalent dose (D_e) distributions: Implications for OSL dating of sediment mixtures. Quaternary Geochronology 4, 204-230.

Arnold, L.J., Bailey, R.M., Tucker, G.E., 2007. Statistical treatment of fluvial dose distributions from southern Colorado arroyo deposits. Quaternary Geochronology 2, 162–167.

Bailey, R.M., Arnold, L.J., 2006. Statistical modelling of single grain quartz D-e distributions and an assessment of procedures for estimating burial dose. Quaternary Science Reviews 25, 2475-2502.

Ballantyne, C.K., Schnabel, C., Xu, S., 2009. Exposure dating and reinterpretation of coarse debris accumulations ('rock glaciers') in the Cairngorm Mountains, Scotland. Journal of Quaternary Science 24, 19-31.

Barre, M., Lamothe, M., 2010. Luminescence dating of archaeosediments: A comparison of K-feldspar and plagioclase IRSL ages. Quaternary Geochronology 5, 324-328.

678 Barsch, D. 1996. Rockglaciers: Indicators for the present and former geoecology in high mountain
679 environments. Springer, Berlin.
680 Bateman, M.D., 2008. Luminescence dating of periglacial sediments and structures. Boreas 37, 574-588.
681 Bearth, P., Heierli, H, Roesli, F., 1987. Geologischer Atlas der Schweiz, Blatt 1237 Albulapass (Atlasblatt
682 81). Schweizerische Geologische Kommission und Landeshydrologie und –geologie (Eds.).
683 Beniston, M., 2005. Mountain climates and climatic change: An overview of processes focusing on the
684 European Alps. Pure and Applied Geophysics 162, 1587-1606.
685 Beniston, M., Diaz, H.F., Bradley, R.S., 1997. Climatic change at high elevation sites: An overview.
686 Climatic Change 36, 233-251.
687 Berthling, I., 2011. Beyond confusion: Rock glaciers as cryo-conditioned landforms. Geomorphology 131,
688 98-106.
689 Bini, A., Buoncristiani, J.F., Couterrand, S., Ellwanger, D., Felber, M., Florineth, D., Graf, H.R., Keller, O.,
690 Kelly, M., Schlüchter, C., Schoeneich, P., 2009. Die Schweiz während des letzteiszeitlichen
691 Maximums (LGM). Map 1:500000. Bundesamt für Landestopographie swisstopo.
692 Böhlert, R., 2010. Reconstructing Lateglacial and Early Holocene Llandscape evolution using a
693 combination of numerical and relative dating methods – Examples from Eastern Switzerland and
694 Eastern France. PhD thesis, University of Zürich, Switzerland.
695 Böhlert, R., Egli, M., Maisch, M., Brandova, D., Ivy-Ochs, S., Kubik, P.W., Haeberli, W., 2011a.
696 Application of a combination of dating techniques to reconstruct the Lateglacial and early Holocene
697 landscape history of the Albula region (eastern Switzerland). Geomorphology 127, 1-13.
698 Böhlert, R., Mirabella, A., Plötze, M., Egli, M., 2011b. Landscape evolution in Val Mulix, eastern Swiss
699 Alps - soil chemical and mineralogical analyses as age proxies. Catena 87, 313-325.
700 Böhlert, R., Compeer, M. Egli, M., Brandová, D., Maisch, M., Kubik, P., 2011c. A combination of relative-
701 numerical dating methods indicates two high Alpine rock glacier activity phases after the glacier
702 advance of the Younger Dryas. The Open Geography Journal 4, 114-130.
703 Bøtter-Jensen, L., Bulur, E., Duller, G.A.T., Murray, A.S., 2000. Advances in luminescence instrument
704 systems. Radiation Measurements 32, 523-528.
705 Castelli, S., 2000. Geomorphologische Kartierung im Gebiet Julierpass, Val Suvretta und Corvatsch
706 (Oberengadin, GR), sowie Versuche zur Relativdatierung der morphologischen Formen mit der
707 Schmidt-Hammer Methode. Diploma thesis, University of Zurich, Switzerland. Unpublished.

708 Coaz, J.W.F., 1850. Blatt XX, Unterabthlg. 2, 1:50,000 (Original Messtischblatt). Archiv-Nr. L+T 468.
709 Schweiz. Eidg. Stabsbureau, Bern.
710 Cossart, E., Fort, M., Didier Bourles, D., Carcaillet, J., Perrier, R., Siame, L., Braucher, R., 2010. Climatic
711 significance of glacier retreat and rockglaciers re-assessed in the light of cosmogenic dating and
712 weathering rind thickness in Clarée valley (Brianconnais, French Alps). Catena 80, 204-219.
713 Duller, G.A.T., 1994. Luminescence dating of poorly bleached sediments from Scotland. Quaternary
714 Science Reviews 13, 521-524.
715 Duller, G.A.T., 2007. Software ANALYST 3.24.
716 Duller, G.A.T., 2008. Single-grain optical dating of Quaternary sediments: why aliquot size matters in
717 luminescence dating. Boreas 37, 589-612.
718 Florineth, D., 1998. Surface geometry of the Last Glacial Maximum (LGM) in the southeastern Swiss Alps
719 (Graubünden) ant its paleoclimatic significance. Eiszeitalter und Gegenwart 48, 23–37.
720 Florineth, D., Schlüchter, S., 2000. Alpine evidence for atmospheric circulation patterns in Europe during
721 the Last Glacial Maximum. Quaternary Research 54, 295–308.
722 Frauenfelder, R., Laustela, M., Kaeaeb, A., 2005. Relative age dating of Alpine rockglacier surfaces.
723 Annals of Geomorphology 49, 145-166.
724 Frauenfelder, R., Hauck, C., Hilbich, C., Kneisel, C., Hoelzle, M. 2008. An integrative observation of
725 kinematics and geophysical parameters of Gianda Grischa rock glacier, Upper Engadine, Swiss Alps.
726 In: Proceedings of the 9th International Conference on Permafrost, University of Alaska, Fairbanks:
727 463-468.
728 Fuchs, M., Lang, A., 2001. OSL dating of coarse-grain fluvial quartz using single-aliquot protocols on
729 sediments from NE-Peloponnese, Greece. Quaternary Science Reviews 20, 783-787.
730 Fuchs, M., Owen, L.A., 2008. Luminescence dating of glacial and associated sediments: review,
731 recommendations and future directions. Boreas 37, 636-659.
732 Gaar, D., Preusser, F., 2012. Luminescence dating of mammoth remains from northern Switzerland.
733 Quaternary Geochronology 10, 257-263.
734 Galbraith, R.F., Green, P.F., 1990. Estimating the component ages in a finite mixture. Nuclear Tracks and
735 Radiation Measurements, 17, 197-206.
736 Galbraith, R.F., Roberts, R.G., Laslett, G.M., Yoshida, H., Olley, J.M., 1999. Optical dating of single and
737 multiple grains of quartz from Jinmium rock shelter, Northern Australia: Part I, experimental design
738 and statistical models. Archaeometry 41 2, 339-364.

739 Haeberli, W. 1985. Creep of mountain permafrost: internal structure and flow of alpine rock glaciers.
740 Mitteilungen der Versuchsanstalt für Wasserbau, Hydrologie und Glaziologie, ETH Zurich, No. 77.
741 Haeberli, W., Hoelzle, M., Kääb, A., Keller, F., Vonder Mühll, D., Wagner, S., 1998. Ten years after
742 drilling through the permafrost of the active rock glacier Murtèl, Eastern Swiss Alps: answered
743 questions and new perspectives. Proceedings of the 7th International Conference of Permafrost,
744 Yellowknife, Collection Nordicana 57, 403-410.
745 Haeberli, W., Brandovà, D., Burga, C., Egli, M., Frauenfelder, R., Kääb, A., Maisch, M., 2003. Methods
746 for absolute and relative age dating of rock-glacier surfaces in alpine permafrost. In: Phillips, M.,
747 Springman, S., Arenson, L. (eds.), Proceedings of the 8th International Conference on Permafrost
748 2003, Zurich. Swets & Zeitlinger, Lisse: 343-348.
749 Haeberli, W., Hallet, B., Arenson, L., Elconin, R., Humlum, O., Kääb, A., Kaufmann, V., Ladanyi, B.,
750 Matsouka, N., Springman, S., Vonder Mühll, D., 2006. Permafrost creep and rock glacier dynamics.
751 Permafrost and Periglacial Processes 17,189-214.
752 Haeberli, W., Noetzli, J., Arenson, L., Delaloye, R., Gärtner-Roer, I., Gruber, S., Isaksen, K., Kneisel, C.,
753 Krautblatter, M., Phillips, M., 2011. Mountain permafrost: Development and challenges of a young
754 research field. Journal of Glaciology 56, 1043-1058.
755 Hamilton, S.J., Whalley, W.B., 1995. Rock glacier nomenclature: A re-assessment. Geomorphology 14,
756 73-80.
757 Heer, A., J., Adamiec, G., Moska, P., 2012. How many grains are there on a single aliquot? Ancient TL
758 30, 9-16.
759 Humlum, O., 1982. Rock glacier types on Disko, Central West Greenland. Geografisk Tidsskrift 82, 59-
760 66.
761 Humlum, O., 1997. Active layer thermal regime at three rock glaciers in Greenland. Permafrost and
762 Periglacial Processes 8, 383-408.
763 Huntley, D.J., Baril, M.R., 1997. The K content of the K-feldspars being measured in optical dating or in
764 thermoluminescence dating. Ancient TL 15, 11 – 13.
765 Huntley, D.J., Lamothe, M., 2001. Ubiquity of anomalous fading in K-feldspars and the measurement and
766 correction for it in optical dating. Canadian Journal of Earth Sciences 38, 1093e1106.
767 Ivy-Ochs, S., Schlüchter, C., Kubik, P.W., Synal, H.A., Beer, J., Kerschner, H., 1996. The exposure ages
768 of an Egesen moraine at Julier Pass, Switzerland, measured with the cosmogenic radionuclides 10Be,
769 26Al and 36Cl. Eclogae Geologicae Helvetiae 89, 1049–1063.

770 Jeong, G.Y., Choi, J.-H., 2012. Variations in quartz OSL components with lithology, weathering and
771 transportation. Quaternary Geochronolog 10, 320-326
772 Kääb, A., 2005. Remote sensing of mountain glaciers and permafrost creep. Physische Geographie 48,
773 University of Zurich, Switzerland.
774 Kääb, A., Haeberli, W., Gudmundsson, G.H., 1997. Analysing the creep of mountain permafrost using
775 high precision aerial photogrammetry: 25 years of monitoring Gruben rock glacier, Swiss Alps.
776 Permafrost and Periglacial Processes 8, 409-426.
777 Kääb, A., Gudmundsson, G.H., Hoelzle M., 1998. Surface deformation of creeping mountain permafrost.
778 Photogrammetric investigations on rock glacier Murtèl, Swiss Alps. Proceedings of the 7th International
779 Permafrost Conference, Yellowknife, Canada. Collection Nordicana, Centre d'études nordiques,
780 Université Laval: 531-537.
781 Krause, W.E., Krbetschek, M.R., Stolz, W., 1997. Dating Quaternary lake sediments from the
782 Schirmacher oasis (East Antarctica) by infra-red stimulated luminescence (IRSL) detected at the
783 wavelength of 560 NM. Quaternary Science Reviews 16, 387-392.
784 Krbetschek, M.R., Götze, J., Dietrich, A. , Trautmann, T., 1997. Spectral information from minerals
785 relevant for luminescence dating. Radiation Measurements 27, 695-748.
786 Kreutzer, S., Schmidt, C., Fuchs, M.C., Dietze, M., Fischer, M., Fuchs, M., 2012. Introducing an R
787 package for luminescence dating analysis. Ancient TL 30, 1-8.
788 Kulig, G., 2005. Erstellung einer Auswertesoftware zur Altersbestimmung mittels Lumineszenzverfahren.
789 BSc thesis, Faculty of Mathematics and Informatics TU Freiberg, Germany (unpublished).
790 Laustela, M., 2003. Messung und Analyse von Verwitterungsrinden zur relativen Altersdatierung
791 ausgewählter Blockgletscher in den Bündner Alpen. Diploma thesis, University of Zurich, Switzerland
792 (unpublished).
793 Laustela, M., Egli, M., Frauenfelder, R., Kaeaeb, A., Maisch, M., Haeberli, W., 2003. Weathering rinds
794 measurements and relative age dating of rockglacier surfaces in crystalline regions of the Eastern
795 Swiss Alps. In: Phillips, M., Springman, S., Arenson, L. (eds.), Proceedings of the 8th International
796 Concerence on Permafrost 2003, Zurich. Swets & Zeitlinger, Lisse: 627-632.
797 Lian, O.B., Roberts, R.G., 2006. Dating the Quaternary: progress in luminescence dating of sediments.
798 Quaternary Science Reviews 25, 2449-2468.
799 Lowick, S.E., Trauerstein, M., Preusser, F., 2012. Testing the application of post IR-IRSL dating to fine
800 grain waterlain sediments. Quaternary Geochronology 8, 33-40.

Maisch, M., 1981. Glazialmorphologische und gletschergeschichtliche Untersuchungen im Gebiet zwischen Landwasser- und Albulatal (Kt. Graubünden, Schweiz). Physische Geographie 3. Dissertation, Department of Geography, University of Zurich, Switzerland.

Matsuoka, N., Ikeda, A., Date, T., 2005. Morphometric analysis of solifluction lobes and rock glaciers in the Swiss Alps. Permafrost and Periglacial Processes 16, 99-113.

Murray, A.S., Wintle, A.G., 2000. Luminescence dating of quartz using an improved single-aliquot regenerative-dose protocol. Radiation Measurements 33, 57-73.

Murray, A.S., Olley, J., 2002. Precision and accuracy in the optically stimulated luminescence dating of sedimentary quartz: A status review. Geochronometria 21, 1-16.

Murray, A.S., Wintle, A.G., 2003. The single aliquot regenerative dose protocol: potential for improvements in reliability. Radiation Measurements 37, 377-381.

Ohlendorf, C., 1998. High Alpine lake sediments as chronicles for regional glacier and climate history in the Upper Engadine, southeastern Switzerland. PhD thesis, ETH Zurich, No. 12705.

Olley, J., Caitcheon, G., Murray, A., 1998. The distribution of apparent dose as determined by optically stimulated luminescence in small aliquots of fluvial quartz: Implications for dating young sediments. Quaternary Geochronology 17, 1033-1040.

Pietsch, T.J., Olley, J.M., Nanson, G.C., 2008. Fluvial transport as a natural luminescence sensitiser of quartz. Quaternary Geochronology 3, 365–376.

Preusser, F., Schlüchter, C., 2004. Dates from an important early Late Pleistocene ice advance in the Aare valley, Switzerland. Eclogae Geologicae Helvetiae 97, 245-253.

Preusser, F., Müller, B.U., Schlüchter, C., 2001. Luminescence dating of sediments from the Luthern Valley, central Switzerland, and implications for the chronology of the last glacial cycle. Quaternary Research 55, 215-222.

Preusser, F., Geyh, M.A., Schlüchter, C., 2003. Timing of Late Pleistocene climate change in lowland Switzerland. Quaternary Science Reviews 22, 1435-1445.

Preusser, F., Ramseyer, K., Schlüchter, C., 2006. Characterisation of low OSL intensity quartz from the New Zealand Alps. Radiation Measurements 41, 871-877.

Preusser, F., Chithambo, M.L., Götte, T., Martini, M., Ramseyer, K., Sendezera, E.J., Susino, G.J., Wintle, A.G., 2009. Quartz as a natural luminescence dosimeter. Earth-Science Reviews 97, 184-214

Steffen, D., Preusser, F., Schlunegger, F. 2009. OSL quartz age underestimation due to unstable signal components. Quaternary Geochronology 4, 353-362.

Suter, J., 1981. Gletschergeschichte des Oberengadins: Untersuchung on Gletscherschwankungen in der Err-Julier-Gruppe. Physische Geographie 2, University of Zurich, Switzerland.

Thomsen, K.J., Murray, A.S., Jain, M., Bøtter-Jensen, L., 2008. Laboratory fading rates of various luminescence signals from feldspar-rich sediment extracts. Radiation Measurements 43, 1474-1486.

Vonder Mühll, D., 1993. Geophysikalische Untersuchungen im Permafrost des Oberengadins. PhD thesis, ETH Zurich, Switzerland, No. 10107.

Wallinga, J., 2002a. Optically stimulated luminescence dating of fluvial deposits: a review. Boreas 31, 303-322.

Wallinga, J., 2002b. On the detection of OSL age overestimation using single-aliquot techniques. Geochronometria 21, 17-26.

Wintle., A.G., 1973. Anomalous fading of thermoluminescence in mineral samples. Nature 245, 143-144.

Figure captions

Fig. 1. Location of the investigated rock glaciers.

Fig. 2. Idealised sequence of rock glacier development (after Haeberli et al., 1998).

Fig. 3. This example shows a tallus-derived rock glacier below a rock wall. The top layer with coarse block approximates the active layer. The blue arrows represent idealised trajectories of single grains subsequently removed at the front for luminescence dating. The measured age theoretically is the time the grain needed to travel this distance within the rock glacier body, protected from daylight. A = rooting zone (grain incorporation); B = rock glacier lobe (grain transport); C = rock glacier front (sampling).

Fig. 4. The rock glaciers sampled for luminescence dating are shown. Sampling locations are represented by red dots. Samples are ideally taken between the coarse blocks on the surface and the eroded and accumulated material at the lower part of the slope. This zone at the rock glacier Gianda Grischa is especially clearly visible as a white band. Digging right below big boulders provides a better slope stability and increases the possible penetration depth (lower right, rock glacier Suvretta). Neighbouring and associated (potentially) inactive and relict creeping forms are indicated by white lines. The dashed line on the rock glacier Gianda Grischa approximates the zone where an older part is

863 overrun by a more active lobe. At this site, three main parts can be distinguished: (A) active rock glacier,
864 (B) older, possibly relict part, (C) inactive rock glacier (based on Frauenfelder et al., 2008).
865
866 Fig. 5. Thermal transfer test for SAL1 K-feldspars comparing three different parameters: preheat
867 temperature (220 °C, 240 °C, 260 °C, 280 °C), optical filters (280 nm, 410 nm, 560 nm) and LED power
868 (90% and 10%).
869
870 Fig. 6. OSL single grain (SG) shine down (left) and dose response curves (right) for samples SAL1 disc1
871 grain 10, SUV3 disc3 grain 2 and 28. Grey value = natural signal.
872
873 Fig. 7. Results from dose recovery tests for single grains (OSL and IRSL) of the rock glacier Salteras.
874 The quartz grains (left) show a clear trend to underestimate the recovery dose (applied dose: 200 s or
875 36.4 Gy). In the case of K-Feldspar (right), a good reproducibility of the luminescence signals can be
876 estimated, as indicated by the low coefficient of variation vDR. N = number of grains.
877
878 Fig. 8. Single grain IRSL shine down curve and dose response curve for K-Feldspar of sample GiG1 and
879 SUV3 and for Plagioclase of sample SAL1. Grey value = natural signal.
880
881 Fig. 9. Equivalent dose distributions of the sample from Salteras using different luminescence methods,
882 top: OSL quartz multiple grain (left) and single grain (right), bottom: IRSL K-feldspar (left) and plagioclase
883 (right). Dose distributions are described by the probability density function (PDF). Statistical analyses
884 include the arithmetic mean (red line), the central age model (CAM, orange line), the minimum age model
885 (MAM, green line) and the finite mixture model (FMM, blue line). vDR = coefficient of variation, N =
886 number of aliquots/grains, sd = standard deviation.
887
888 Fig. 10. Equivalent dose distributions of samples from Suvretta comparing OSL (top) and IRSL (bottom)
889 measurement results. Dose distributions are described by the probability density function (PDF).
890 Statistical analyses include the arithmetic mean (red line), the central age model (CAM, orange line), the
891 minimum age model (MAM, green line) and the finite mixture model (FMM, blue line). N = number of
892 aliquots/grains, sd = standard deviation.
893

Fig. 11. Equivalent dose distributions of samples from Gianda Grischa showing results of IRSL measurements. Dose distributions are described by the probability density function (PDF). Statistical analyses include the arithmetic mean (red line), and for sample GiG 2 additionally the central age model (CAM, orange line), the minimum age model (MAM, green line) and the finite mixture model (FMM, blue line). N = number of aliquots/grains, sd = standard deviation.

Figure1

Click here to download high resolution image

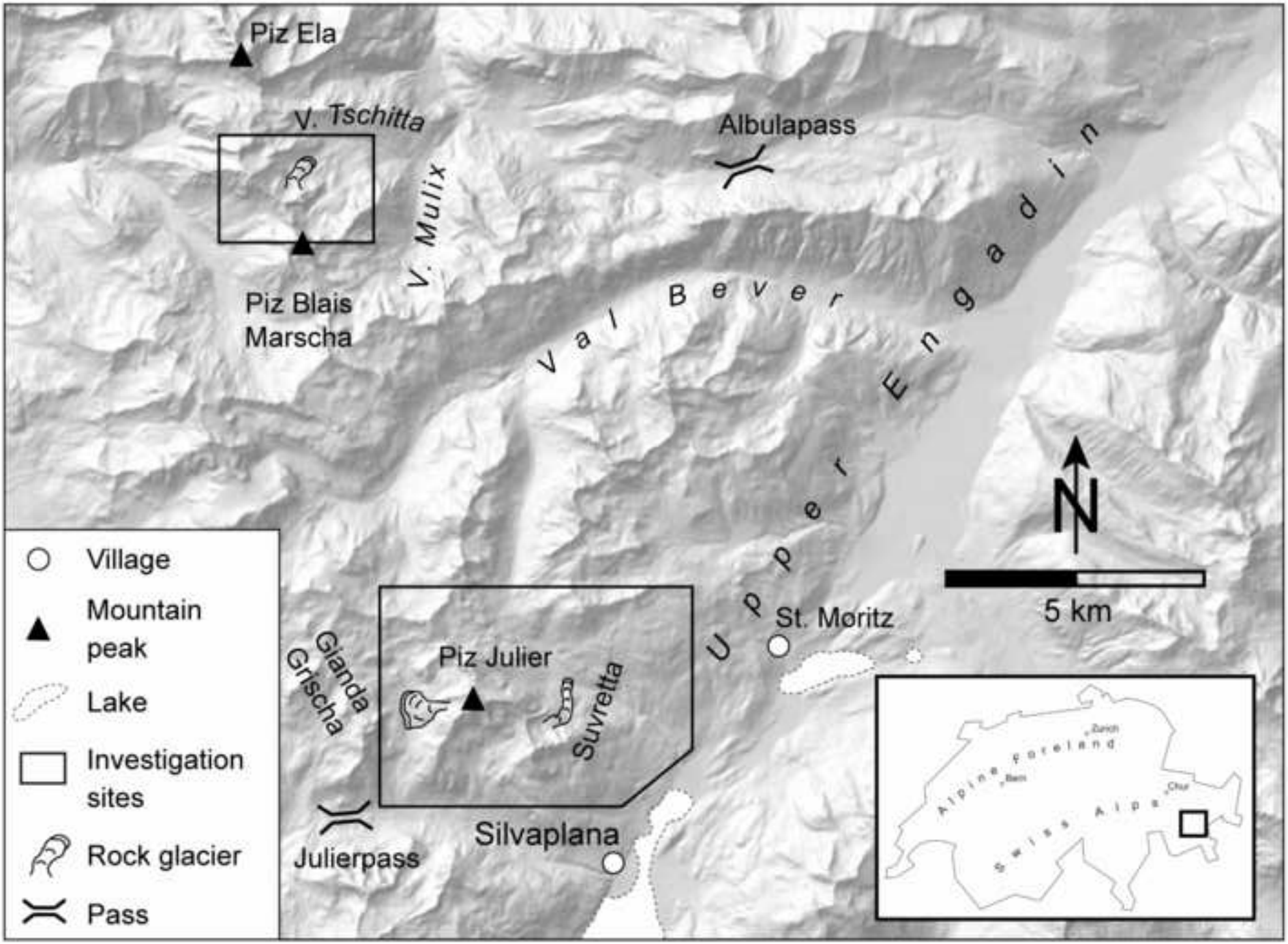

Figure2_greyscale
Click here to download high resolution image

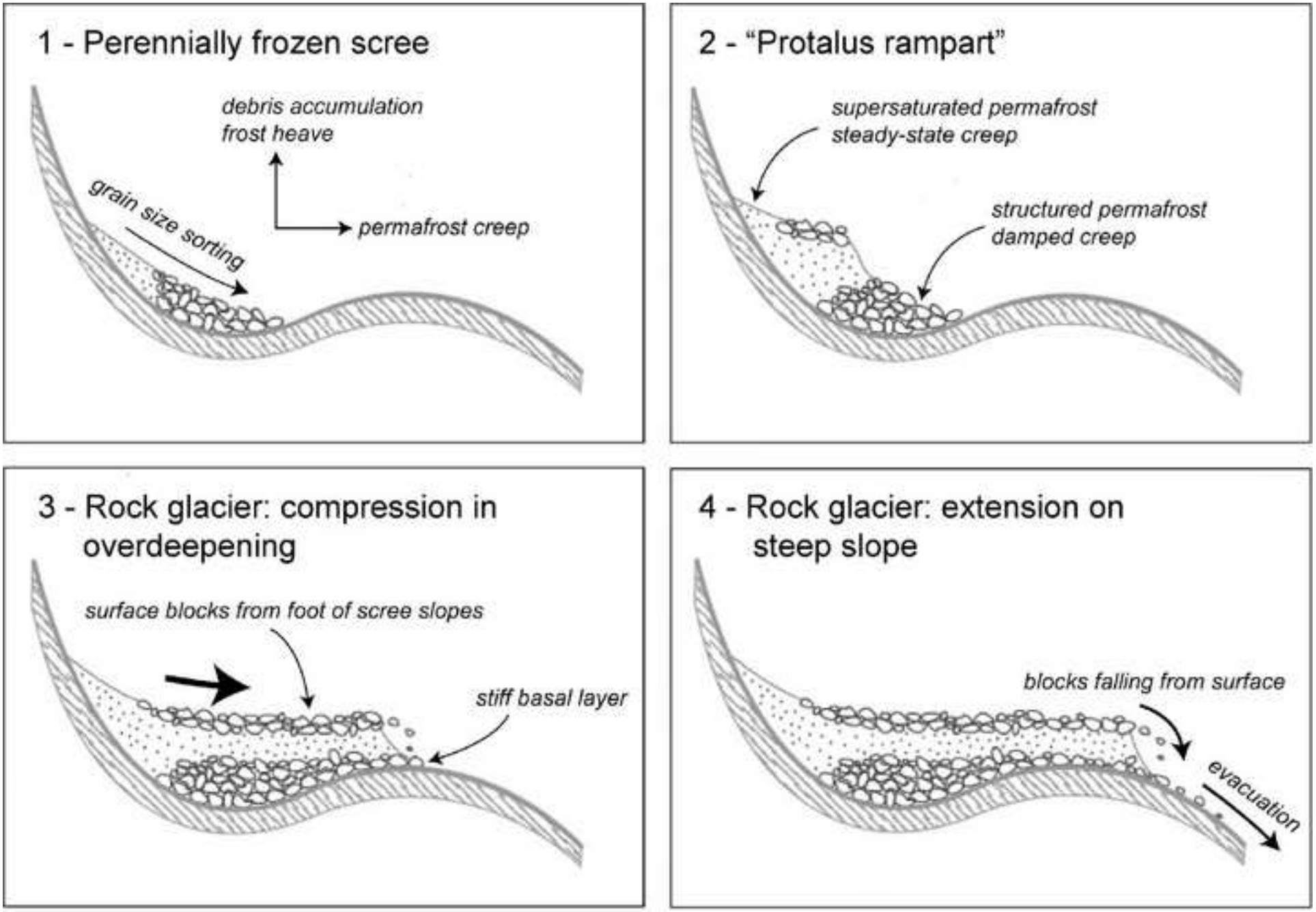

Figure3_colour

Click here to download high resolution image

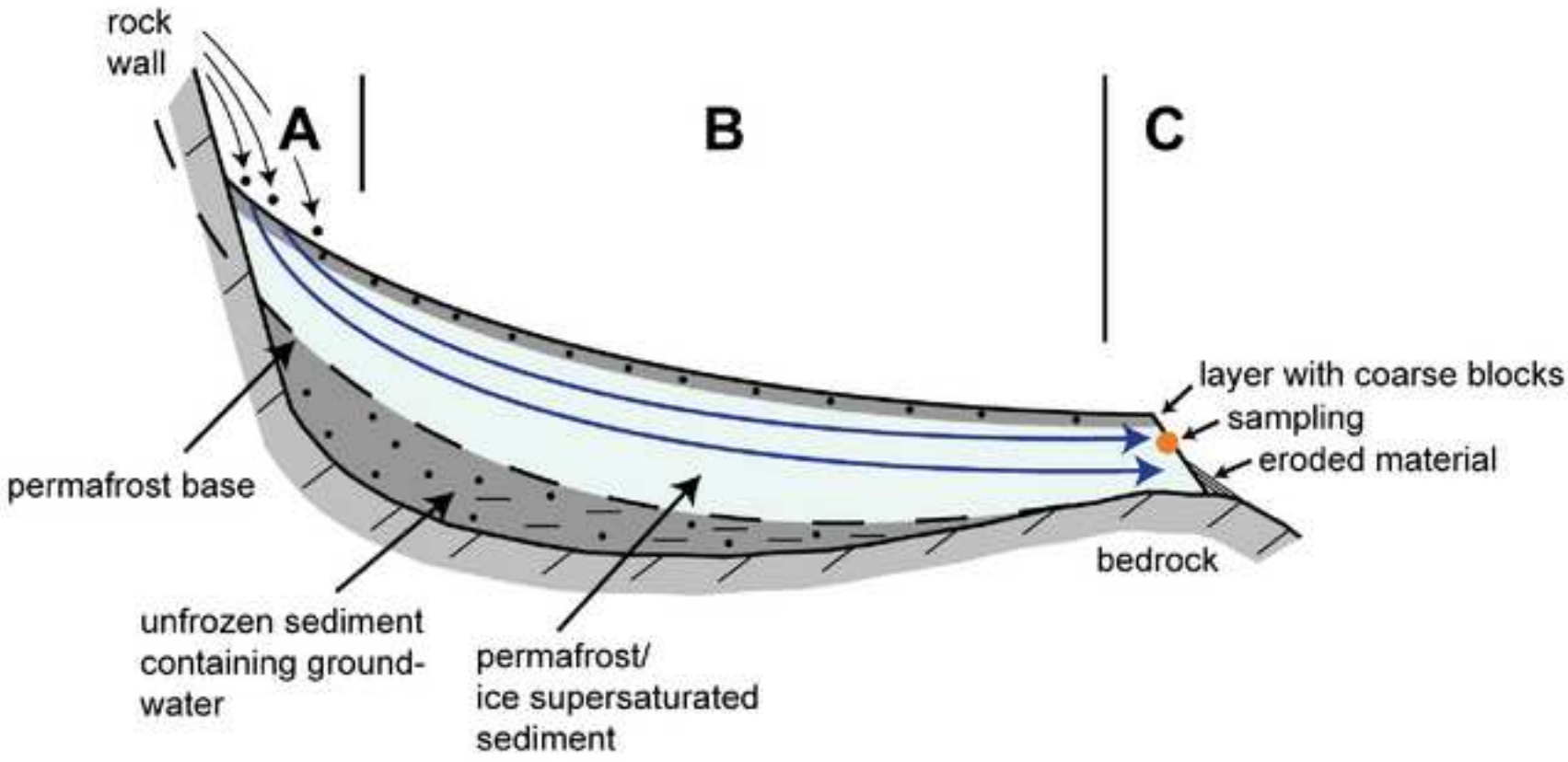

Figure4_colour

Click here to download high resolution image

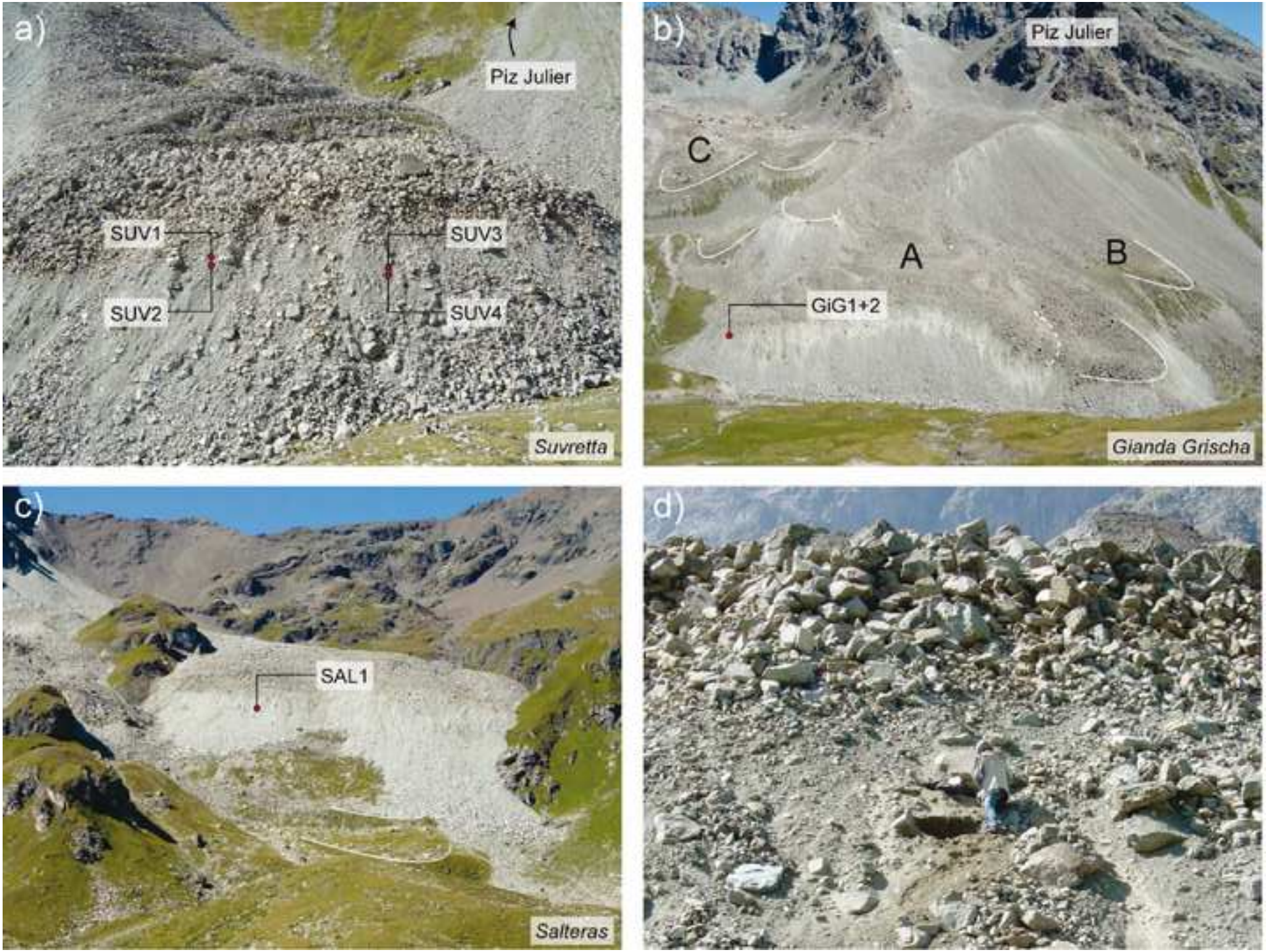

Figure5_greyscale
Click here to download high resolution image

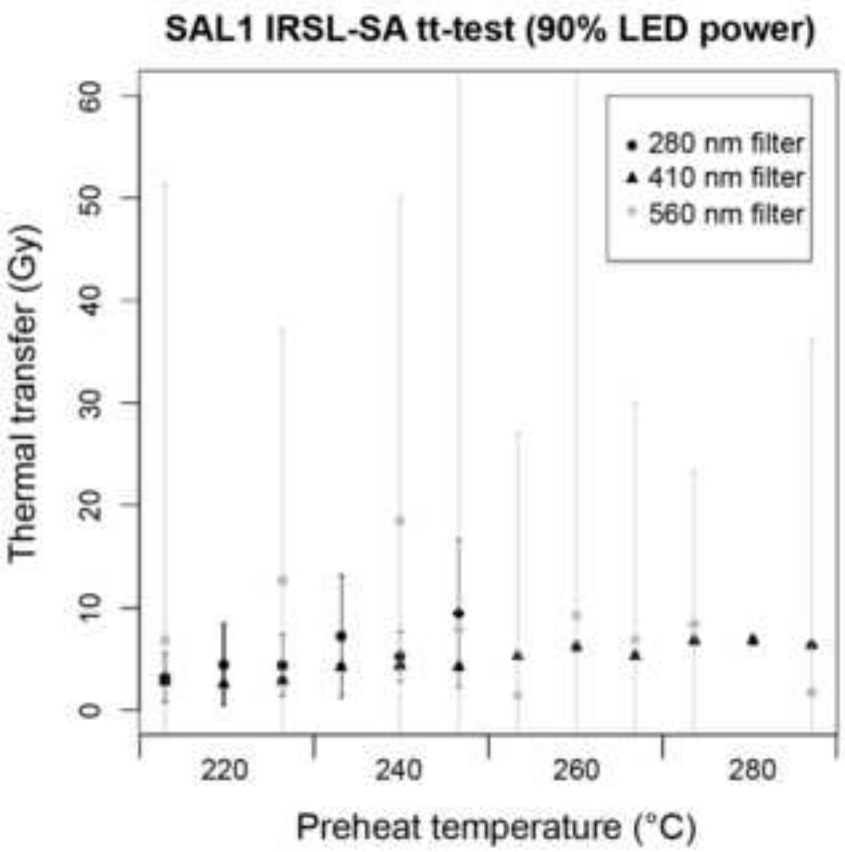

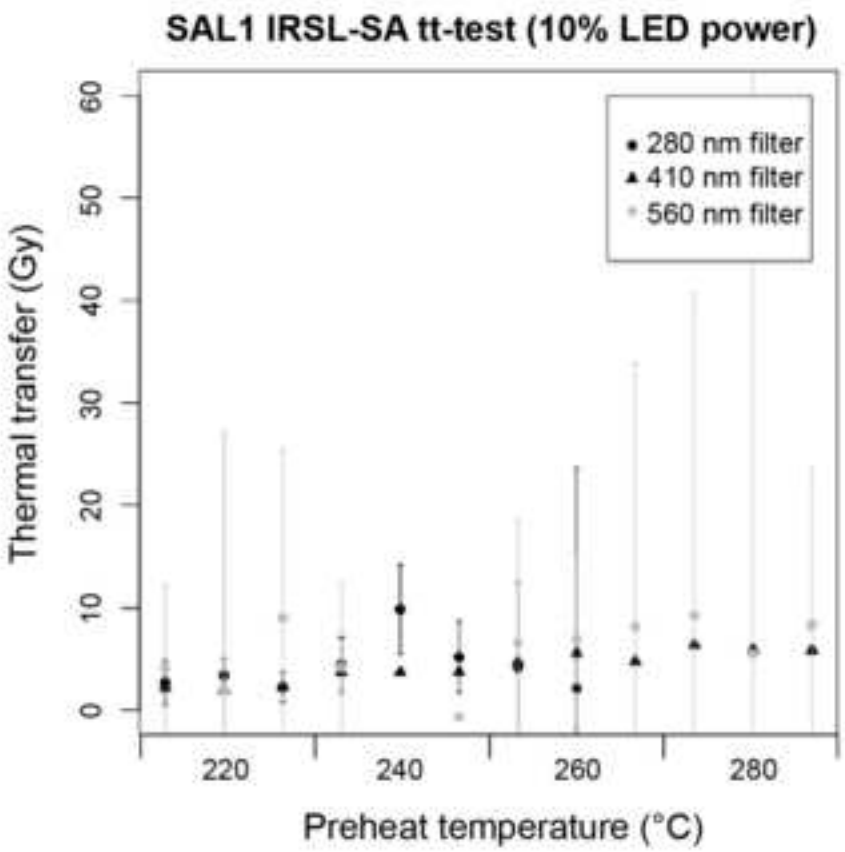

Figure6_greyscale

Click here to download high resolution image

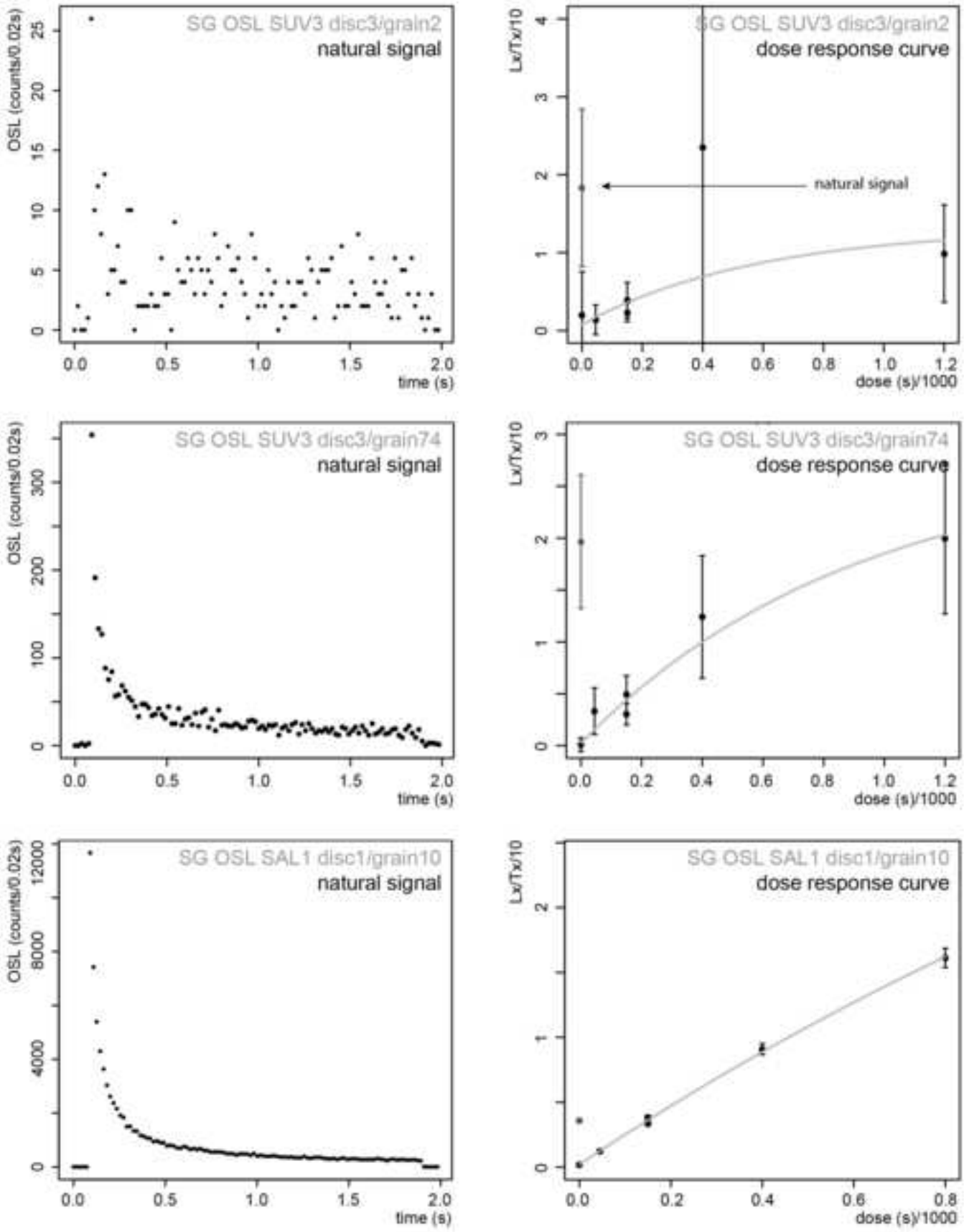

Figure7_greyscale
Click here to download high resolution image

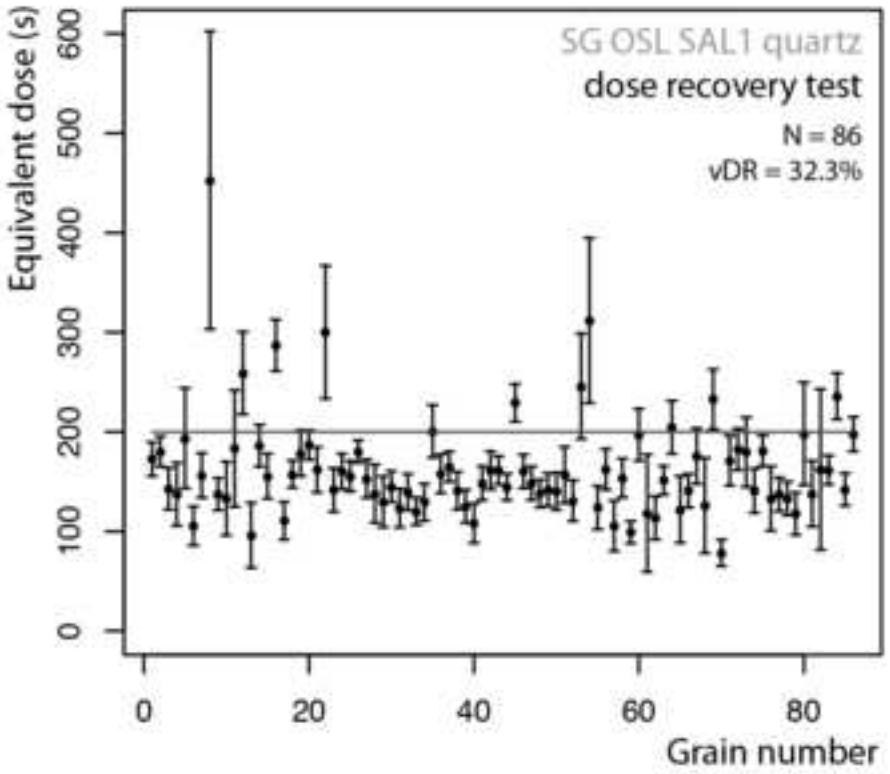

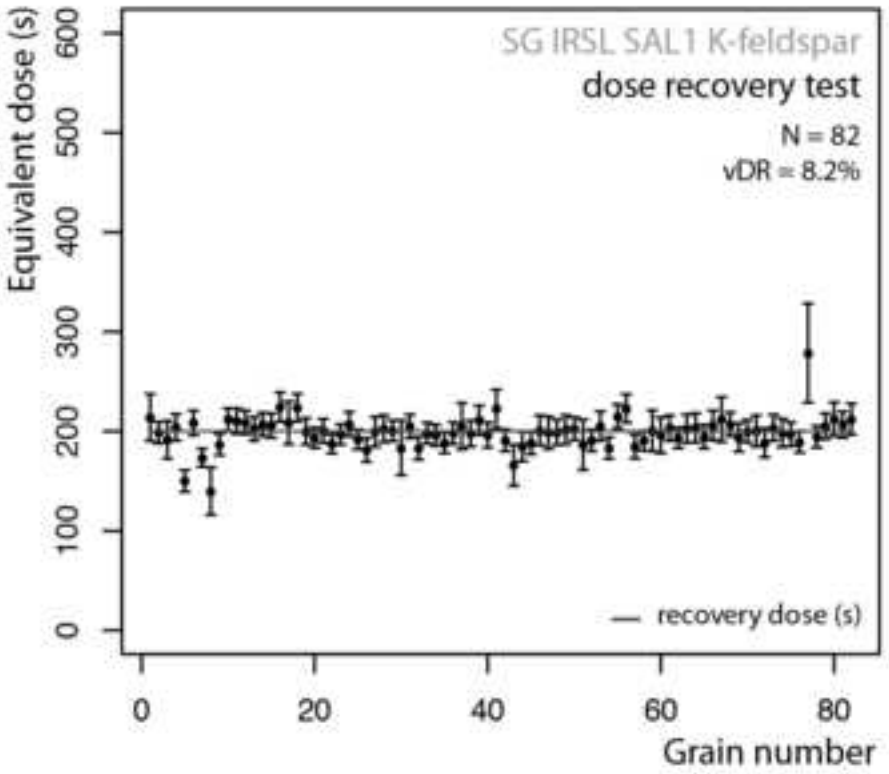

Figure8_greyscale

Click here to download high resolution image

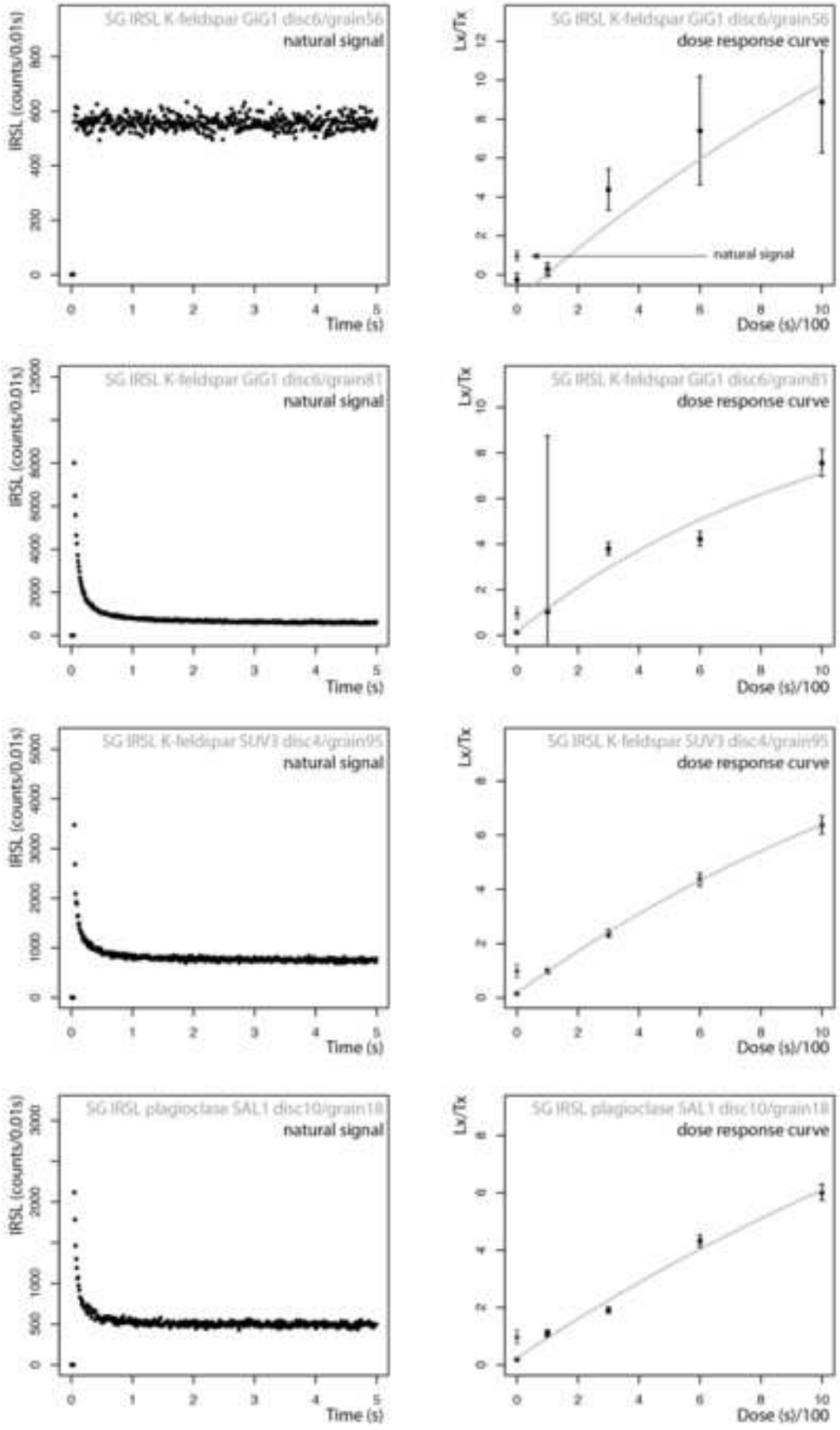

Figure9_colour

Click here to download high resolution image

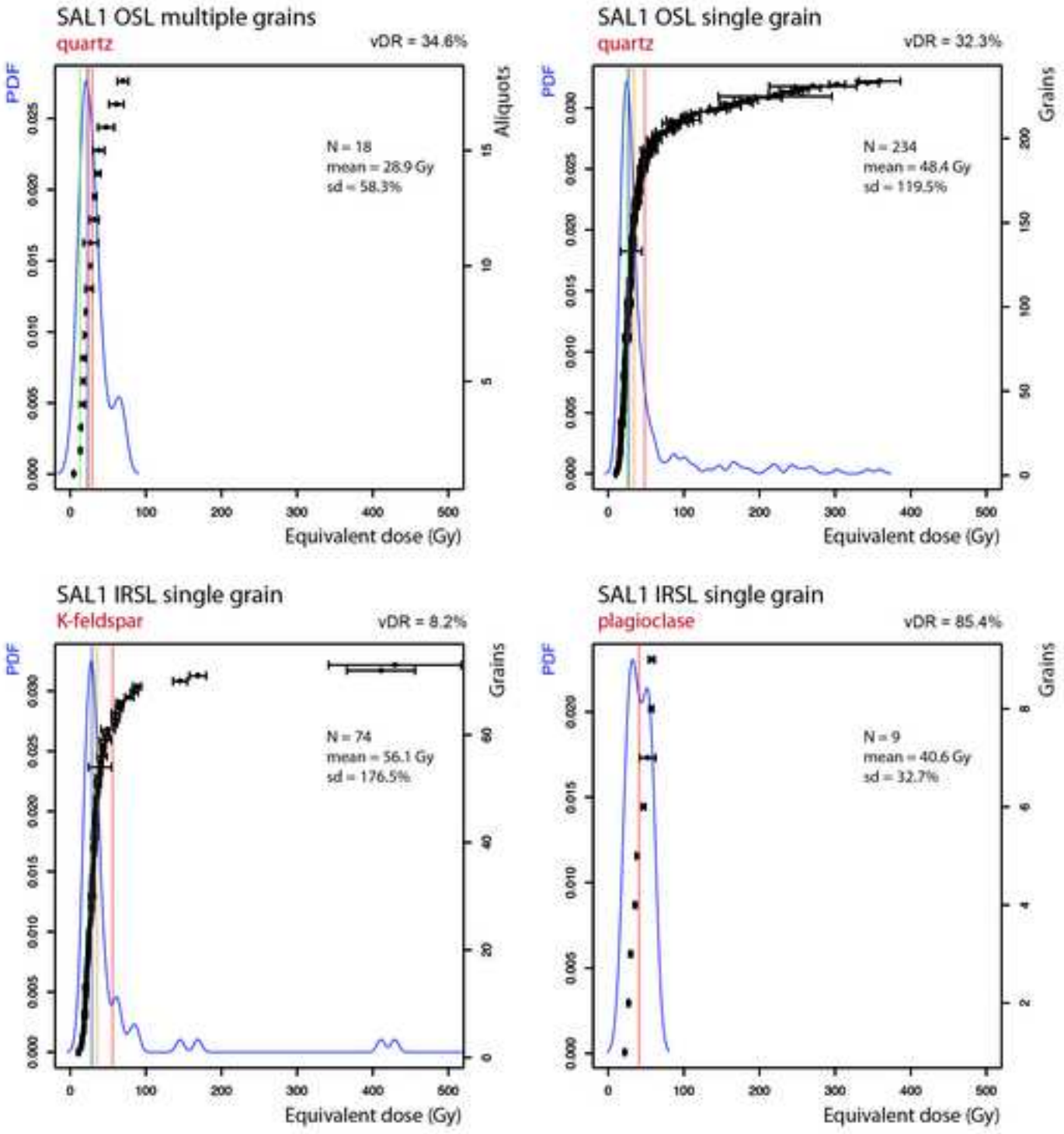

Figure10_colour
Click here to download high resolution image

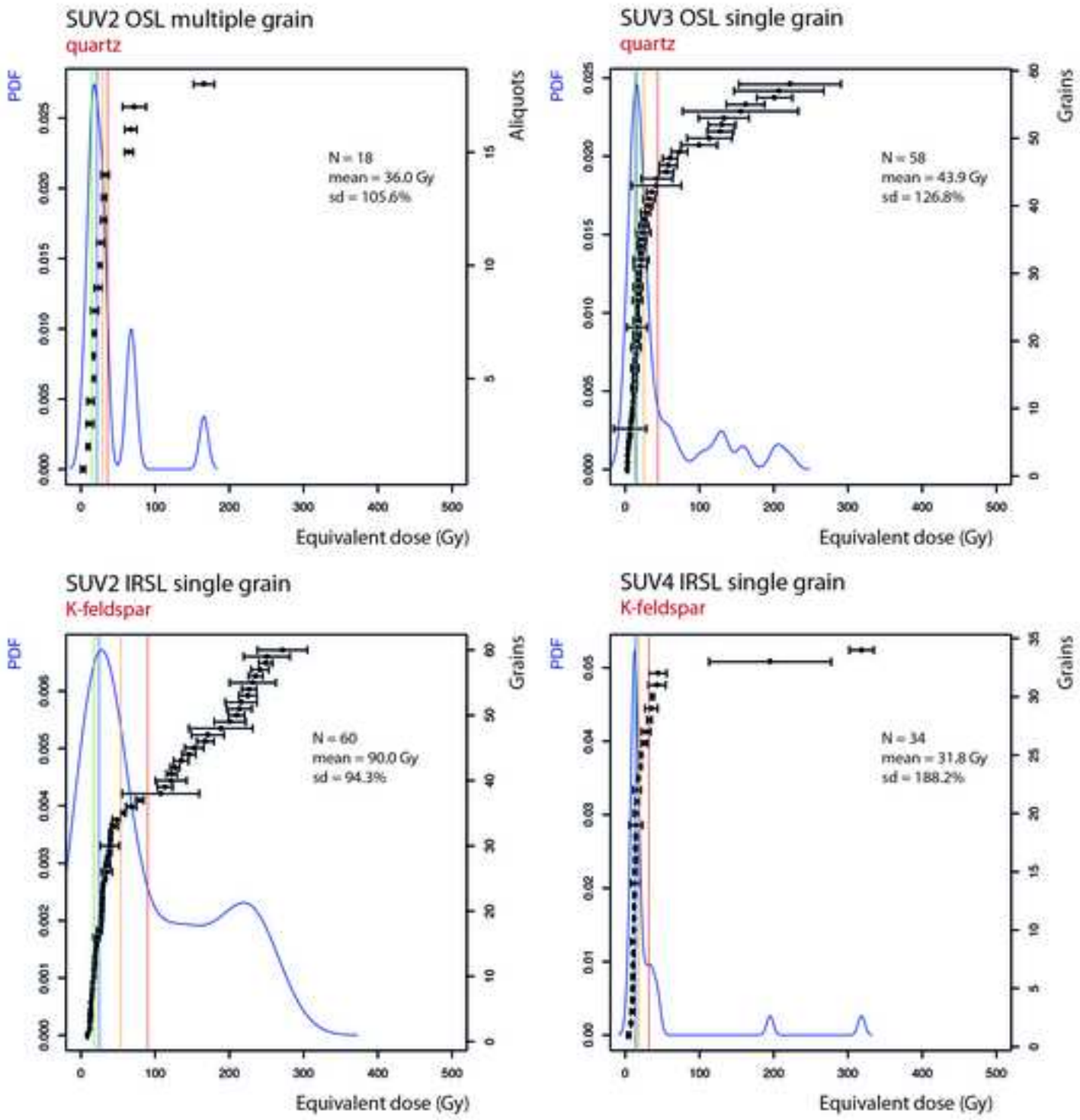

Figure11_colour

Click here to download high resolution image

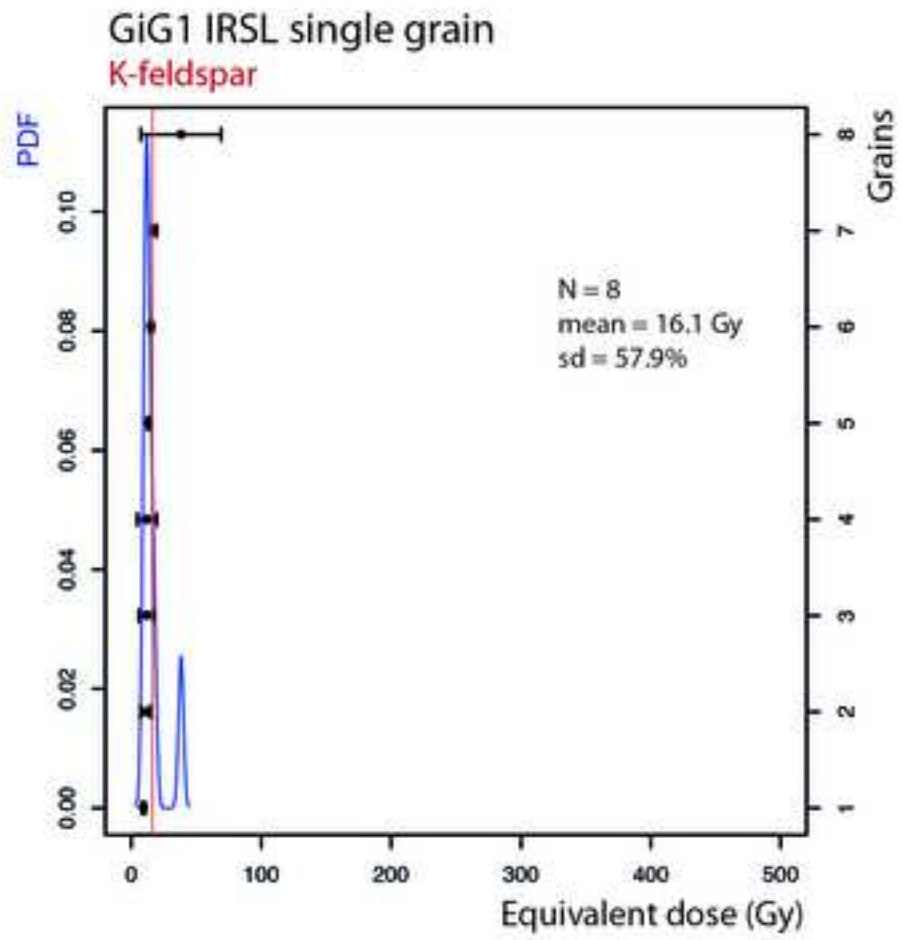

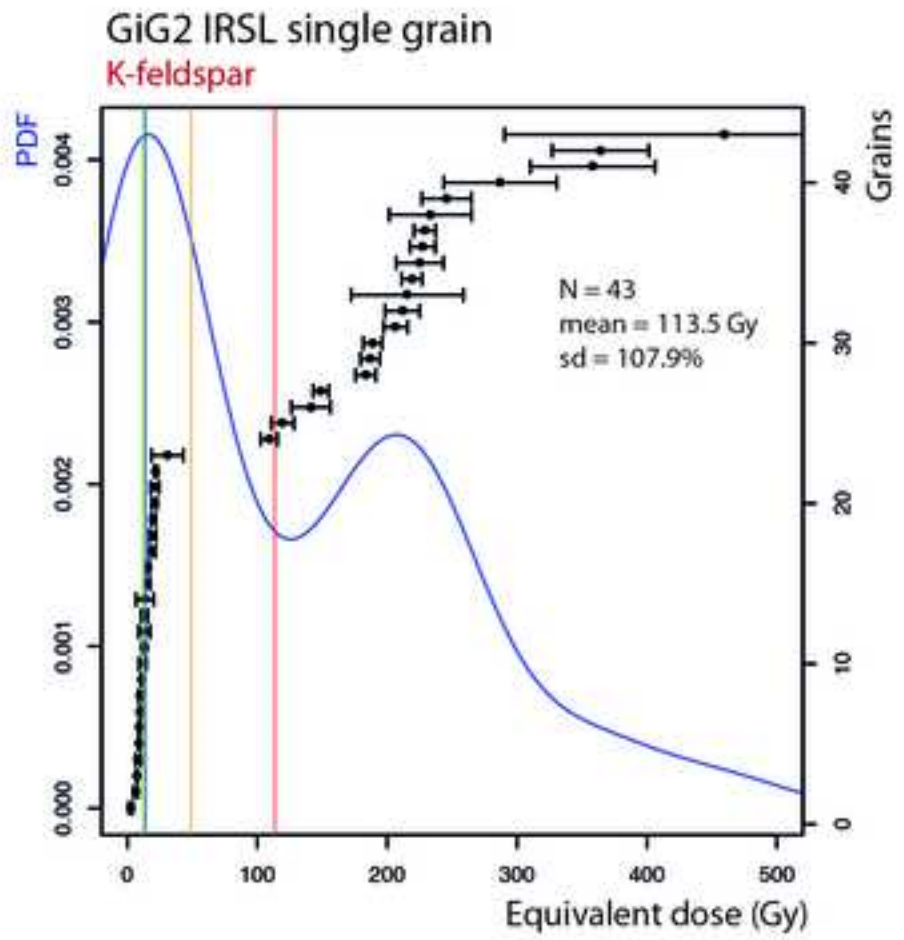

Table 2

Table 2. Data for dose rate estimation (SAL = Salteras; SUV = Suvretta; GiG = Gianda Grischa; D_{cos} = cosmic dose rate; I = in situ S = saturation; U = used for calculations)

Sample	Radionuclides			D_{cos}	Water content			External
	^{238}U (Bq ka^{-1})	^{232}Th (Bq ka^{-1})	^{40}K (Bq ka^{-1})	(mGy ka^{-1})	I (%)	S (%)	U (%)	Dos rate (Gy ka^{-1})
SAL1	28.5 ± 0.7	29.2 ± 1.4	911.1 ± 3.7	144	4.6	15.7	12 ± 8	3.5
SUV1	69.8 ± 1.4	45.6 ± 2.0	761.3 ± 2.9	190	2.5	9.0	10 ± 8	4.1
SUV2	74.7 ± 1.6	45.6 ± 2.1	774.5 ± 3.2	190	4.5	15.9	12 ± 8	4.2
SUV3	77.0 ± 6.0	45.5 ± 2.0	770.0 ± 50.0	171	4.4	16.6	12 ± 8	4.3
SUV4	77.0 ± 5.0	46.5 ± 2.0	750.0 ± 50.0	171	4.6	44.4	25 ± 20	3.8
GiG1+2	52.0 ± 4.0	36.5 ± 2.0	705.0 ± 40.0	250	3.4	18.0	12 ± 9	3.6

Table 1

Table 1. Potential processes related rock glaciers and their effects on the luminescence signals

Process	Effect
Deposition and incorporation	
Aeolian input onto rock glacier surface	Supply of well-bleached grains
Input from short distance transport (e.g., from mass movements)	Insufficient light exposure (Incomplete bleaching)
Grain retention on rock glacier surface (e.g., due to snow cover)	Prolonged light exposure, well bleached grains
Internal source of fine material (grain size reduction by permafrost)	No or insufficient light exposure (Partial bleaching)
Basal material uptake (incorporation of older sediments)	No or insufficient light exposure (Incomplete bleaching)
Transport	
Horizontal sediment mixing (e.g., by meltwater)	Mixing with younger grains
Vertical sediment mixing (e.g., crevasses)	Mixing with grains, e.g., derived from aeolian material supplied to the rock glacier surface
Trajectories of individual grains (grain transport at constant depth?)	Uncertainties related to shielding against light exposure as well as cosmic dose rate
Permafrost variability	Uncertainties in dose rate efficiency and paleo-water/ice content

Table 3

Table 3. Palaeodose estimates and luminescence ages determined for different approaches. MG = multiple-grain aliquots; SG = single grains; kf = K-feldspar; pl = plagioclase; n = number of included aliquots/grains; Mean = arithmetic mean; RSD = relative standard deviation; CAM = Central Age Model; od(CAM) = overdispersion corresponding to CAM; FMM = Finite Mixture Model; Comp 1-3: proportion of each component determined by the FMM; Age = calculated only for samples with n > 15 using the component of highest proportion of the FMM.

Sample	Method	n	Mean (Gy)	RSD (%)	CAM (%)	od(CAM)	FMM (Gy)	Comp 1 (%)	Comp 2 (%)	Comp 3 (%)	Age (ka)
Salteras											
SAL1	OSL-MG	18	28.9 ± 4.0	58.3	24.2 ± 3.7	0.56	22.8 ± 3.8	5.7	76.0	18.3	6.4 ± 1.2
SAL1	OSL-SG	234	48.4 ± 3.8	119.5	34.3 ± 1.6	0.68	26.9 ± 0.8	84.2	8.1	7.7	7.7 ± 0.7
SAL1	IRSL-SG (kf)	74	56.1 ± 11.5	176.5	35.9 ± 3.0	0.68	28.6 ± 1.5	85.3	10.7	4.0	6.4 ± 0.6
SAL1	IRSL-SG (pl)	9	40.6 ± 4.4	32.7	-	-	-	-	-	-	-
Suvretta											
SUV1	OSL-SG	3	206.3 ± 65.6	55.1	-	-	-	-	-	-	-
SUV2	OSL-MG	18	36.0 ± 8.7	105.6	29.5 ± 5.5	0.66	21.8 ± 3.0	78.4	21.6	-	5.2 ± 0.8
	OSL-SG	1	29.3 ± 2.5	-	-	-	-	-	-		-
	IRSL-SG (kf)	60	90.0 ± 10.9	94.3	54.0 ± 7.4	1.03	24.7 ± 1.6	59.5	40.5	-	4.8 ± 0.5
SUV3	OSL-SG	58	43.9 ± 7.5	125.8	25.2 ± 3.6	0.94	14.9 ± 1.4	73.9	26.1	-	3.5 ± 0.5
	IRSL-SG (kf)	9	11.4 ± 6.5	170.5	-	-	-	-	-	-	-
SUV4	OSL-SG	3	11.7 ± 3.5	51.6	-	-	-	-	-	-	-
	IRSL-SG (kf)	34	31.8 ± 10.3	188.2	18.3 ± 2.7	0.72	13.9 ± 1.6	79.6	15.7	4.7	3.0 ± 0.6
	IRSL-SG (pl)	1	20.7 ± 4.4	-	-	-	-	-	-	-	-
Gianda Grischa											
GiG1	OSL-SG	5	145.1 ± 29.8	46.0	-	-	-	-	-	-	-
	IRSL-SG (kf)	8	16.1 ± 3.6	62.8	-	-	-	-	-	-	-
GiG2	OSL-SG	2	133.8 ± 13.5	14.2	-	-	-	-	-	-	-
	IRSL-SG (kf)	43	113.5 ± 18.5	106.6	49.2 ± 11.2	1.42	13.4 ± 1.2	53.1	46.9	-	3.0 ± 0.4

Supplementary Data

Click here to download Supplementary Data: RG_supplementary_FMM-vs-OD.pdf